

Recent Progress of Heterojunction Ultraviolet Photodetectors: Materials, Integrations, and Applications

Jiixin Chen, Weixin Ouyang, Wei Yang, Jr-Hau He,* and Xiaosheng Fang*

Ultraviolet photodetectors (UV PDs) with “5S” (high sensitivity, high signal-to-noise ratio, excellent spectrum selectivity, fast speed, and great stability) have been proposed as promising optoelectronics in recent years. To realize high-performance UV PDs, heterojunctions are created to form a built-in electrical field for suppressing recombination of photogenerated carriers and promoting collection efficiency. In this progress report, the fundamental components of heterojunctions including UV response semiconductors and other materials functionalized with unique effects are discussed. Then, strategies of building PDs with lattice-matched heterojunctions, van der Waals heterostructures, and other heterojunctions are summarized. Finally, several applications based on heterojunction/heterostructure UV PDs are discussed, comprising flexible photodetectors, logic gates, and image sensors. This work draws an outline of diverse materials as well as basic assembly methods applied in heterojunction/heterostructure UV PDs, which will help to bring about new possibilities and call for more efforts to unleash the potential of heterojunctions.

1. Introduction

It has been widely accepted that UV radiation has a profound effect on the development of production and the improvement of the quality of our life, for instance, overexposure to UV rays can lead to sunburn, skin cancer, and other potential problems.^[1] UV photodetectors that convert UV illumination into electric signals are fundamental optoelectrical components which have unique requirements for “5S” (sensitivity, selectivity, stability, signal-to-noise ratio, and response speed).^[2] To that end, it is a common strategy to construct heterojunctions for reducing carrier recombination, which can suppress the PD's photoresponse to high-energy photons. Generally, heterojunctions applied in photodetectors are formed between two kinds of semiconductors, or a semiconductor and a conductor


(metals or conductive carbon materials). For UV photodetectors, normally one of the two materials is responsible for photon absorption and the other helps to form the junction. The creation of a heterojunction where charges are separated, suppresses photocarriers recombination at the interfaces to optimize photodetection with higher responsivity, quantum efficiency, and photogain.^[3–5]

Presently, the researches on perovskites,^[6–11] graphene,^[12] and other materials^[2,13–16] are emerging in an endless stream and these materials with excellent properties can be used for heterojunction UV PDs. Perovskites are a good choice for optoelectronic devices because of their tunable bandgaps, large extinction coefficient, and so on. It has been confirmed that the excellent match in the conduction band of perovskite-TiO₂ junctions can effectively promote charge separation.^[17,18] The heterostructure between MAPbI₃ quantum dots (QDs) and TiO₂ shows a relative fast and stable response to UV light, and the combining also enhances the long-term stability of perovskite MAPbI₃.^[7] Another example is the heterojunctions between graphene and wide-bandgap semiconductors. Combining wide-bandgap semiconductors and graphene, which possesses high carrier mobility and high transparency, is very useful for deep ultraviolet detection. The rectifying effect between graphene and semiconductors such as GaN and Ga₂O₃ leads to promoted responsivity and sensitivity of solar blind ultraviolet detectors.^[19,20] These materials have brought diverse choices of light absorption part of a heterojunction/heterostructure, and provided more methods for enhanced photodetection performance.

Heterojunctions used to be produced by combining semiconductors with different bandgap energies but closely matched lattice parameters.^[21] Above the influence of interface defects and surface states, lattice-matched heterojunctions can achieve high separation efficiency and easy transport of photogenerated electron–hole pairs. For example, type II Se/Si heterojunctions with matched lattice own a very small dark current for high sensitivity.^[22] Such assembling needs strong chemical bonds that are not easy to achieve, while in van der Waals (vdWs) heterostructures, different materials are assembled physically through weaker vdWs force.^[23] VdWs integration frees heterojunction growth from strict requirements of similar lattice characteristics and electrical properties. Therefore, it provides a flexible method that is possible to combine materials with different structures and properties.^[24]

J. X. Chen, Dr. W. X. Ouyang, W. Yang, Prof. X. S. Fang
Department of Materials Science
Fudan University
Shanghai 200433, P. R. China
E-mail: xshfang@fudan.edu.cn

Prof. J.-H. He
Department of Materials Science and Engineering
City University of Hong Kong
Kowloon, Hong Kong SAR 999077, P. R. China
E-mail: jrhaue@cityu.edu.hk

 The ORCID identification number(s) for the author(s) of this article can be found under <https://doi.org/10.1002/adfm.201909909>.

DOI: 10.1002/adfm.201909909

In addition, 2D materials-based vdWs heterostructure has come to the foreground in recent years. TMDs,^[25] graphene,^[26] etc., are used in some PDs for ultrahigh responsivity and detectivity. However, lots of materials are not able to create vdWs junctions due to poor surface roughness that keeps two materials too far to build vdWs interactions, let alone atomically sharp interfaces and electronically abrupt junctions. But the hybrid still presents typical junction behaviors. They are also playing an important role in UV photodetection.

Hence, we are keen to review this concept of a heterojunction UV photodetector to enhance the response by combining two or more components.

In the first part of this report, much attention is paid to materials in various kinds of heterojunctions/heterostructures. These materials are divided into two parts: one is the major photosensitive component of a heterojunction that responds to light (such as ZnO), while the other component functionalized with some unique effects helps to form a built-in electric field. In the second part, we discuss different types of heterojunction/heterostructure UV PDs in terms of the integration ways, specifically, the interaction strength between the two components. It should be noted that we are mainly concerned about the enhanced performance of PDs without giving too much attention to the origin of interface interactions. In the third part, we give a brief description about applications based on heterojunction UV PDs. Several representative flexible UV PDs are listed including image sensors and logic circuits constructed on heterojunctions. What follows are a final summary and a glimpse of future heterojunction UV PDs.

2. Materials for Heterojunction UV PDs

For the materials utilized in building UV PDs, the most common candidate materials are UV active materials. The formed heterojunction between these materials can regulate the behaviors of photoinduced charge carriers, leading to improved UV photoresponse.

In a heterojunction UV PD, if one material is set as UV active materials, the other materials may also have response to visible or even infrared light. Under UV irradiation, photoinduced charge carriers can be generated in both materials. With the help of inner electric fields, these charge carriers can be efficiently separated and transported to electrodes, leading to enhanced UV photoresponse. While under visible irradiation, only the materials with a narrow bandgap can generate photoinduced charge carriers. However, the hindrance of non-responsive materials greatly increases the recombination possibilities of photogenerated electrons and holes, which results in poor visible photoresponse.

If the heterojunctions are formed by two narrow bandgap materials with response to visible or even infrared light, the as-fabricated heterojunction PDs can exhibit broadband photoresponse, in which UV response can be enhanced because of the formed electric field at interfaces. To realize UV selective detection, UV-pass filters can be equipped to eliminate the influence of visible photoresponse.

There are also some specific situations. If one material is up/down converters, they can convert UV irradiation into visible or deep UV irradiation. If the converted irradiation can be harvested and detected by the other material, the heterostructure

constructed by these two materials can also exhibit UV photoreponse (more on this next).

2.1. Semiconductors with UV Response

Semiconductors with UV response are principal to a heterojunction UV photodetector. These semiconductors can be divided into inorganic materials with different conduction types, organic materials, and organic–inorganic hybrid materials. Specially, few-layer 2D materials with wide bandgaps might also exhibit UV response, showing great potentials in heterojunction UV photodetectors.

2.1.1. n-Type Inorganic Semiconductors

Most sensitive materials for UV photodetector are inorganic semiconductors with a large bandgap and strong UV absorption. Plenty of the common active materials exhibit n-type conductivity, and the majority of UV photodetectors are based on n-type semiconductors.^[27] In general, n-type metal oxide semiconductors are commonly used building blocks in photoelectric devices because of their specific electronic and optoelectronic properties.^[28–30] With suitable bandgap, unique electric properties, and confined carrier conduction pathways, their low-dimensional nanostructures are suitable for sensitive materials in photoelectric devices. Moreover, the ease of preparing metal oxide semiconductor nanostructures makes them promising for assembling high-performance UV PDs in large scale.^[31] For example, common binary metal oxides with a wide bandgap such as ZnO,^[32] TiO₂,^[33] and SnO₂^[34] have been widely investigated and applied in UV PDs. Meanwhile, ternary metal oxides such as Zn₂SnO₄,^[35] Zn₂GaO₄,^[36] Zn₂GeO₄,^[37,38] and MgZnO^[39] have also been reported for their applications in UV PDs.^[40] **Figure 1a** shows a photodetector based on Zn₂GeO₄ nanorods and it presents moderate photoresponse under UV light illumination. Besides, the bandgaps of multielement metal oxide semiconductors can be tuned by alternating the stoichiometric ratios of different atoms, suggesting that their derivatives are good choices for broadband photodetectors.

Notably, ZnS, a wide-bandgap metal sulfide semiconductor (≈ 3.72 eV for cubic zinc blende and ≈ 3.77 eV for hexagonal wurtzite), is considered as an arising star for photodetection because of its good electron mobility, moderate charge transport ability, and high transmittance toward visible light.^[41] ZnS has a large direct bandgap corresponding to the UV region, making it a good choice for a UV-responsive visible-blind semiconductor. In addition, ternary sulfide Ga₂In₄S₉ is also an n-type semiconductor exhibiting great potential in UV detection. Through a controllable chemical vapor deposition (CVD) growth process, ultrathin 2D Ga₂In₄S₉ with long carrier lifetime and long minority carrier diffusion length can be synthesized.^[42]

2.1.2. p-Type Inorganic Semiconductors

Different from n-type semiconductors with electrons as the majority carriers, the majority carriers of p-type semiconductors

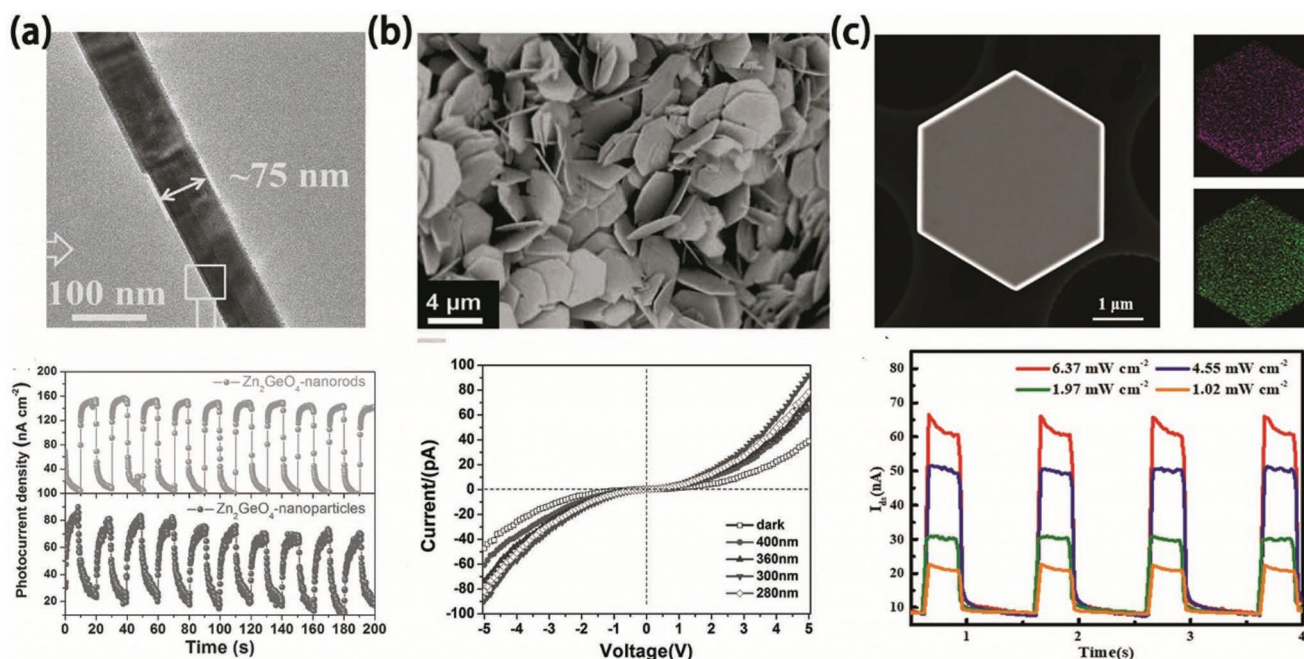


Figure 1. a) Image of Zn_2GeO_4 nanorods and their on/off photocurrent responses under UV (254 nm) light. Reproduced with permission.^[40] Copyright 2016, Wiley-VCH. b) Typical SEM image of CuGaO_2 nanoparticle film and current–voltage (I – V) curves of the $\text{CuGaO}_2/\text{ZnS}$ device under 280, 300, 360, and 400 nm illumination and dark conditions. Reproduced with permission.^[47] Copyright 2017, Wiley-VCH. c) TEM image of 2D PbI_2 and current–time (I – t) measurement at $V_{\text{ds}} = 5$ V on PbI_2 -based photodetector under different power densities of a 375 nm laser. Reproduced with permission.^[73] Copyright 2019, Wiley-VCH.

are holes originating from the defects in the crystal.^[2] Diamond is introduced as the representative of single-element p-type materials applied in photodetection. Due to its wide bandgap, high breakdown voltage, high carrier mobility, high radiation tolerance, high dark resistance, and low self-noise, diamond has become one of the most interesting candidates for the next-generation photodetectors used in the spectral range from UV to X-rays.^[43]

Binary-element SiC and GaN can be p-type semiconductors and they have been applied as sensitive materials in commercial photodetecting devices. Silicon carbide (SiC) with a bandgap of 2.4–3.3 eV has developed as one of the most important wide-bandgap materials of UV photodetection. p-Type SiC-based photodetectors can achieve solar-blind photodetection with fast speed and high signal-to-noise ratios.^[44] With a large direct bandgap of 3.4 eV, gallium nitride (GaN) is another outstanding material for visible-blind UV detection because of its large light absorption coefficient, high saturation-electron drift velocity (310 cm s^{-1}), good thermal and chemical stability, and remarkable tolerability of harsh environments.^[45] The superior mechanical properties and chemical stability make SiC and GaN devices ideal UV photodetectors while working in harsh environments.

As a typical binary p-type metal oxide semiconductor, NiO has a wide direct energy bandgap in the range of 3.2–3.8 eV. Due to its low cost, earth abundance, visible light blindness, large excitonic binding energy, and wide bandgap, NiO can be a superior candidate for UV photodetectors utilized in the environment surrounded with inevitable thermal energy.^[46]

CuGaO_2 and BiOCl are representative ternary-element p-type metal oxide semiconductors applied in UV photodetectors.^[31,47] Delafossite CuGaO_2 , as a p-type material with a

hybrid orbit for holes to transport driven by sp hybridization between $3d^{10}$ of Cu^+ ion and $2p$ of two O^{2-} , has emerged as an excellent p-type material for UV photodetection due to its large bandgap (≈ 3.6 eV) and good transparency.^[48] Figure 1b displays a photodetector based on CuGaO_2 nanoplate/ ZnS microsphere film. The heterostructure shows a higher UV absorption and enhanced photoresponse properties. Bismuth oxide halides (BiOX ($X = \text{Cl}, \text{Br}, \text{and I}$)) have a layered structure, which consists of tetragonal $[\text{Bi}_2\text{O}_2]^{2+}$ positive slabs interleaved by double negative slabs of halide atoms along the c -axis.^[49] The layered structure provides a space large enough to polarize the related atoms and orbitals. The induced dipole separates the electron–hole pair efficiently, which is beneficial for enhancing photocatalytic activity and photoconductivity.^[50] Depending on diverse preparation methods, the bandgap of BiOCl varies from 3.0 to 3.5 eV, which makes BiOCl nanostructures suitable for UV-A light detection.^[51] However, these BiOCl -based UV photodetectors suffer from poor conductivity and low photoresponse.^[52] More efforts should be paid to overcome these deficiencies.

2.1.3. Organic Materials

Due to the small mass, low cost of fabrication, and easy processing compared with inorganic counterparts, UV photodetectors based on organic materials especially small molecular materials and polymers, have thrived rapidly. Materials such as 2-(1,10:30100-triphenyl-50-yl)-9,9-diphenyl-9H-fluorene (TPF) and (9,9-diphenyl-9H-fluoren-2-yl)diphenylphosphine oxide (DFPPO) are provided with higher electron mobility and feasible level alignment.^[53] UV photodetectors based on polymers such

as tris-(8-hydroxyquinoline) gadolinium (Gdq)^[54] and poly(5,7-bis(4-decanyl-2-thienyl)-thieno(3,4-b)diathiazole-thiophene-2,5) (PDDTT)^[55] present fast response and high sensitivity. These organic materials have flourished for UV photodetectors. Because of their specific qualities including relatively short excited state lifetime, intense phosphorescence emission, high thermal stability, and excellent charge transport ability, tricarboxyl di-imine rhenium complexes and more organic materials have also been adopted in highly sensitive UV photodetectors.^[56]

2.1.4. Organic–Inorganic Hybrids

Perovskites with unique electrical and optoelectronic properties are representative organic–inorganic hybrids.^[57] Worldwide researchers' attention has been paid on perovskites to producing broad applications of light-emitting diodes (LEDs), optically pumped lasers, photoelectrochemical (PEC) cells, and photodetectors.^[6] The direct bandgap nature, high light absorption ability, and wide-range light absorption of perovskites make them suitable candidates for photodetectors with broadband photoresponse.^[8] The short conduction pathway for photogenerated charge carriers ensures the related photoelectric devices with fast response speed. Moreover, very low concentration of defects and traps in perovskites greatly reduces charge carrier recombination.^[58] These characteristics strongly recommend the organic–inorganic hybrid perovskites as ideal building blocks for high-performance PDs. Perovskites with different structures (polycrystalline film,^[9] single crystal,^[10] and low-dimensional nanostructure^[59]) have been synthesized. Together with various device configurations, perovskites-based devices demonstrate unprecedented progress in photodetecting performance.^[60] In preliminary research, common perovskites such as CH₃NH₃PbI₃ and CsPbI₃ are generally narrow-bandgap semiconductors and they exhibit broadband photoresponse.^[61] With the extended investigations on perovskites, some perovskites with wide bandgaps such as methyl ammonium lead chloride (MAPbCl₃)^[62,63] and (PEA)₂PbBr₄ (C₆H₅CH₂CH₂NH₃⁺, PEA⁺)^[64] single crystals are transparent to visible but sensitive to UV radiation, which are recognized as promising candidates for UV photodetectors.

2.1.5. New Trends

2D materials, which feature a layered structure weakly bonded by vdWs forces in atomic or molecular thickness and infinite planar dimensions, are easy to prepare and transfer. 2D materials with tunable bandgaps from 0 to 6 eV are sensitive over a wide range of the electromagnetic spectrum. They are recognized as useful items with remarkable electronic, photonic, and mechanical properties and are deemed the research focus in the next few decades.^[65–68] The commonly investigated 2D materials such as MoS₂, WS₂, and MoSe₂ always exhibit broadband photoresponse (especially visible-light response) because of their narrow bandgaps. Limited by the availability of wide-bandgap 2D semiconductors, the progress of UV photodetectors based on 2D materials is restricted.^[69,70] However, the newly investigated 2D materials of GeSe₂,^[71] Sr₂Nb₃O₁₀,^[11]

and GeS₂^[72] have shown bandgap of about 3 eV, and they have been fabricated into UV photodetectors showing competitive photoresponse with state-of-the-art UV detectors. As a typical 2D layered semiconductor, the Pb and I atoms of PbI₂ are covalently bonded within each plane and the planes are stacked together by weak vdWs force (Figure 1c). As its layer number changes, the bandgap of a PbI₂ nanoflake varies from 2.38 to 2.5 eV. With a direct bandgap and a higher light absorbance capability, multilayered PbI₂ is favorable for constructing UV photodetectors.^[73]

Thanks to the advance of micro/nanofabrication technologies, more 2D nanostructures shall be produced and their fascinating properties will facilitate the enhancement of related PDs.

2.2. Materials Functionalized with Specific Effects

Photoconductive-type UV photodetectors based on single semiconductor always suffer from relatively high dark current and slow response speed because of the surface defect states. Constructing heterojunctions can effectively deal with these deficiencies. To achieve improved photodetection, metal nanoparticles with localized surface plasmon resonance (LSPR) effect, QDs and nanocrystals with multiple exciton generation effect, and down/upconverters can be utilized in a heterojunction to enhance the light absorption, thus increase the generation of photoinduced charge carriers.

Carbon materials, organic materials, and other appropriate semiconductors can form heterojunctions with UV response semiconductors to achieve more efficient separation and transport of charge carriers. These modifications have positive influence on the carrier behaviors in heterojunctions, resulting in superior UV photodetection.

2.2.1. Localized Surface Plasmon Resonance Effect

The photoexcitation-induced collective oscillations of free charges confined in a highly conductive nanocrystal are described as LSPR.^[74] In recent years, metal nanocrystals (such as Au, Ag, Pt, Bi, and Cu) with LSPR effects have been extensively investigated for their intriguing optical properties and versatile technological applications. The light absorption of these metal nanostructures can be tailored over a broad spectral range from UV to infrared by tuning the size, shape, metal composition, and environment.^[75] Due to the light-confinement effect and tunable light absorption, various plasmonic PDs combine low-dimensional semiconductor nanostructures and these plasmonic metal nanocrystals have demonstrated excellent plasmon-enhanced device performance, for instance, by sputtering Au nanoparticles, the responsivity of Se can be largely enhanced in a wideband range (Figure 2a).^[76]

The decay of resonant surface plasmon can generate a nonradiative way and the resulted additional scattering and relaxation of these high-energy carriers produce photocurrents in PDs.^[77] The bandgap of semiconductor is no longer the determining factor for the generation of hot carriers as usual, the Schottky barrier height or tunnel junction becomes the leading factor,

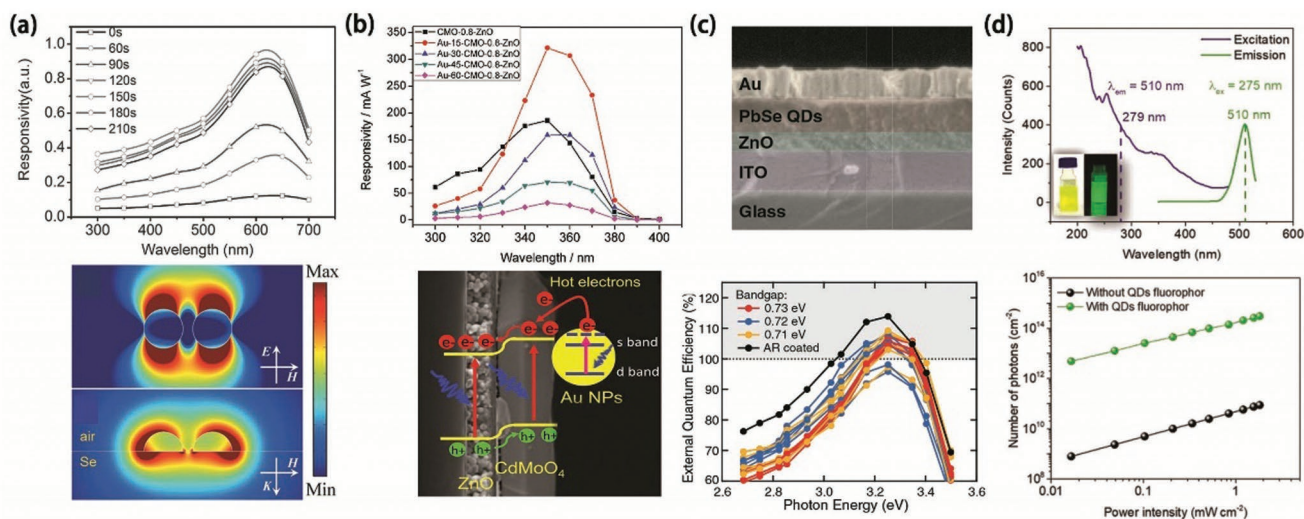


Figure 2. a) Spectral responsivity of Se photodetectors with various Au sputtering times under 2 mA current (bias = 5 V) and spatial distribution of the electric field intensity of Au NPs with the diameter of 40 nm and the interspace gap of dimer of 10 nm at the wavelength of 600 nm. Reproduced with permission.^[76] Copyright 2016, Wiley-VCH. b) Spectral response and proposed mechanism for the improved photoelectric performance of the Au NPs-decorated CdMoO₄-ZnO photodetectors at 5 V bias. Reproduced with permission.^[29] Copyright 2017, Wiley-VCH. c) Cross-sectional SEM and EQE peaks of a typical PbSe quantum dot film solar cell device. Reproduced with permission.^[79] Copyright 2011, American Association for the Advancement of Science. d) PL emission and excitation spectra of the CsPbBr₃ QDs and the inset shows the photo of as-prepared CsPbBr₃ QDs solution in cyclohexane under white light or UV light illumination. And the calculated number of photons arrived at the perovskite surface with (lower) and without down conversion by QDs fluorophore. Reproduced with permission.^[84] Copyright 2019, Wiley-VCH.

making it possible to detect photons with energies lower than the bandgap of semiconductors. The hybrid metal–semiconductor system can function as plasmonic PDs. The geometry of plasmonic nanostructures, the composition of plasmonic material, and the interface conditions of plasmonic materials and semiconductors can have great influence on the hot-carrier processes, the regulation of which can be achieved by the precise control of these factors, which can be confirmed by the CdMoO₄/ZnO heterojunction modified with Au nanoparticles (Figure 2b).^[29] The deeper exploration and utilization of the hot electron injection effect would lead to modified optoelectronic performance. Furthermore, the direct coupling of electronic excitations of optical energy through plasmon resonance can achieve enhanced photogain and selectivity in various optoelectronic applications.

2.2.2. Multiple Exciton Generation Effect

In common, a photon excitation can produce only one electron–hole pair at once and the conversion efficiency from photons to electron–hole pairs can hardly reach a hundred percent. However, upon the absorption of a single photon that bears at least twice the bandgap energy, semiconductor nanocrystals or QDs with multiple exciton generation effect will generate more than one pair of electron–hole.^[78] Moreover, after the photoexcited electrons are trapped at the QD surface, long-lived holes are left behind and circulate through the photoconductor and the external circuit multiple times before recombining with electrons. Thus, the conversion efficiency can exceed 100%.^[79] The multiple exciton generation process in these systems is an instantaneous event that finishes within 200 fs. Besides, these

nanocrystals or QDs also possess semiconducting property which enables construction of heterojunctions with semiconductors.^[80] As presented in Figure 2c, the combination of metal oxides with PbSe QDs with this multiple exciton generation effect should result in greatly improved EQE of the device.^[81,82]

2.2.3. Down/Upconversion

The coupling between new structural concepts and optoelectronic applications based on up/downconverters is of great significance.^[83] It can achieve light harvesting in the long (short) spectral range and the extended photon up (down)-conversion range under sunlight irradiation to achieve maximum energy conversion. Thus, these up/downconverters can be used to construct UV heterojunction photodetector without the participation of semiconductors with UV response. CsPbBr₃ QDs can be prepared as a fluorophore and applied to solar-blind UV light detection. By integrating as-fabricated all-inorganic CsPbBr₃ QDs, the photodetection system exhibits an enhanced detection for UV-C light (279 nm), which is mainly due to the increased number of photons irradiated on the perovskite absorber layer by over three orders of magnitude via downshifting the UV-C light into visible light (Figure 2d).^[84]

2.2.4. Photovoltaic Effect

Photovoltaic effect can take place in the hybrid of carbon materials, organic materials, and other appropriate semiconductors with UV response semiconductors. Originated from the photovoltaic effect, the as-formed electric field at the interfaces can

promote the separation and transport of photoinduced charge carriers, leading to improved photoresponse and response speed of related PDs.

Conductive Carbon Materials: Conductive carbon materials such as graphene, activated carbon, and carbon nanotubes, are a suitable option for UV PDs owing to their superior optical and electric properties.

Graphene is a one-atom-thick planar structure of carbon atom and its discovery has led the research of 2D materials. Up to now, there are extensive graphene-/graphene oxides-based applications in photodetection. Owing to the high carrier mobility, the preceding investigations of graphene have demonstrated its metallic conductivity, which can separate the photogenerated electron–hole pairs effectively.^[85] What's more, zero-bandgap 2D graphene-based photodetector usually exhibits UV–vis–IR photoresponse. In addition to their good environmental stability, tunable work function, and mature processing technique, graphene and its derivative have been adopted as one important component in vdWs heterostructures assembling.^[15] The hybridization of graphene with semiconductors may not only compensate for graphene's intrinsic weakness and fully exploit its potential to new special functions, but also serve as a general strategy for enhancement of hybrid photodetecting system.^[86,87]

Because of their unique band structure, excellent electronic and optoelectronic properties, and super mechanical and chemical stabilities, carbon nanotubes (CNTs), another important allotrope of carbon, are preferred in optoelectronics. A flexible and thorn-like ZnO-multiwalled carbon nanotubes (MWCNTs) hybrid paper with high aspect ratio is designed for efficient UV-sensing application. The photodetector fabricated from the hybrid paper demonstrates a high sensitivity and fast transient response to UV light, which is attributed to efficient carrier transport and collection of the hybrid paper. These fascinating properties make it advantageous to assemble a low-cost and flexible CNT-based photodetector with high quantum efficiency, high sensitivity, and high speed.^[88]

Organic Materials: With the advantages of easy fabrication, broadband absorption range, and elastic modulating of their semiconductor characteristics, p-type organic materials are very suitable for photodetection.^[89] The hybrid PDs based on p-type organic molecules with tunable functionality and n-type inorganic semiconductors with superior intrinsic carrier mobility, usually present high photodetecting performance, thanks to the efficient separation and transfer of photoinduced charge carriers resulting from the p–n heterojunctions. Various kinds of organic materials, such as polyaniline (PANI),^[90] poly(vinyl alcohol) (PVA),^[91] poly(acrylonitrile) (PAN),^[27] poly(vinyl carbazole) (PVK),^[92] polypyrrole (PPy),^[93] and even pyrene-tricyanofuran derivatives,^[94,95] are also adopted to modify the photoelectric properties of semiconductor-based PDs.^[96]

Semiconductors: Heterojunctions formed between different semiconductors have profound influences on the electronic properties and present potentials in multifunction and property tuning, these as-built heterostructures have been extensively applied in solar cells, PEC cells, photodetectors, and other photovoltaic devices. It has been broadly reported that the built-in electric field formed at the heterostructure interface,

can efficiently separate photogenerated electron–hole pairs and regulate the transport of carriers in photoelectric devices.^[97] Referring to the different conduction types of semiconductors, this kind of heterojunctions can be classified into n–n, p–n, and p–i–n generally.^[47,98,99]

A majority of UV response semiconductors utilized in heterojunctions present n-type conduction behaviors, the detailed description of heterojunction built between n-type semiconductors has been frequently summarized in other reviews,^[2,31,100] the related contents will not be mentioned in this section. This part intends to concentrate on the heterojunctions formed between UV response semiconductors and other semiconductors that are categorized according to the numbers of constitution elements.

1) *Single elemental semiconductor:* p-type single-element semiconductors comprise group III (boron), group IV (silicon, germanium, and several carbon materials), group V (phosphorus), and group VI elemental semiconductors (α -sulfur, selenium, and tellurium). Here, some representative elemental semiconductors applied in UV PDs are presented.

With an estimated bandgap of 1.5 eV, a theoretical high conductivity ($\approx 10^2 \Omega^{-1} \text{ cm}^{-1}$), and a high carrier mobility ($10^2 \text{ cm}^2 \text{ V}^{-1} \text{ s}^{-1}$), 2D boron nanosheet is an elemental p-type semiconductor with potential as a UV–vis broadband photodetection material.^[101,102] **Figure 3a** shows morphology and device performance of a typical photodetector based on 2D boron and as-fabricated photodetector displayed moderate photoresponse under 325 nm light illumination. What researchers can do with adopting is that the high responsivity is from its high crystallinity. The single-crystalline boron nanosheets with high quality are prepared by a vapor-solid process and it can realize large-scale production. In addition, 2D boron has been combined with semiconductors to form heterojunction UV photodetector.^[103,104]

Single-wall carbon nanotubes (SWCNTs) can be either semiconducting or metallic, depending on their geometrical characteristics. By changing its diameter and chirality, the bandgap of semiconducting SWCNTs can be tuned. Semiconducting SWCNTs not only present ultrahigh carrier mobility, ballistic transport, and superior mechanical flexibility, but also exhibit strong broadband light absorption (peak absorptivity $> 10^5 \text{ cm}^{-1}$), fast light response up to picoseconds, and Ohmic contact with electrodes.^[105] Graphene nanoribbons (GNRs) are narrow stripes of graphene, where quantum confinement effect may induce a bandgap in the electronic structure. Bandgap can be adjusted by varying the edge shape and width of GNR.^[106]

Graphdiyne (GD) possesses both sp and sp² carbons with two diacetylenic linkages between the adjacent carbon hexagonal structures and exhibits an electronic conductivity of $2.56 \times 10^{-1} \text{ S m}^{-1}$. It is promising for the optoelectronic and photocatalytic applications because of its large specific area, high hole mobility, and semiconducting behavior with a calculated bandgap of 0.47 and 1.12 eV.^[107] GD:ZnO nanocomposites are applied in the assembly of UV photodetectors. It is demonstrated that the junction formed between the GD and ZnO nanoparticles greatly promotes the carrier-exchange process, and hence significantly enhances the photoresponse.^[108]

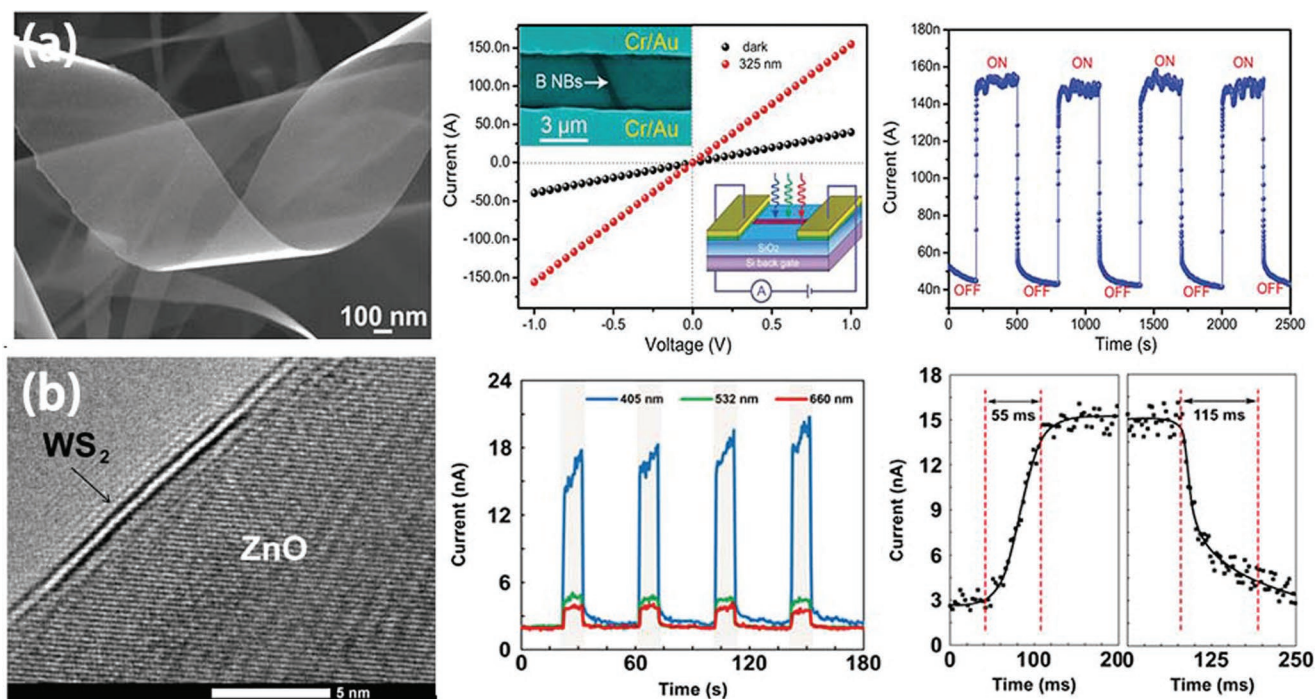


Figure 3. a) Typical SEM image of ultrathin boron nanosheets and I - V as well as I - t curves for this photodetector under 325 nm light. Reproduced with permission.^[102] Copyright 2015, Wiley-VCH. b) TEM image and on-off measurements of a ZnO/WS₂ nanowire. Test conditions: at 1 V bias and under 0.5 W cm⁻² illumination of 405, 532, and 660 nm. Reproduced with permission.^[132] Copyright 2018, American Chemical Society.

As a stable layered structure allotrope of phosphorus, widely studied group V semiconductor black phosphorus (BP) is found to show bipolar conduction behaviors and achieves very high carrier mobility up to ≈ 1000 cm² V⁻¹ s⁻¹.^[109,110] The bandgap of bulk BP is about 0.3 eV. After exfoliated to monolayer BP, its bandgap is calculated to be 1.5 eV, demonstrating its light detection ability from UV to visible region.^[111] Considering its specific properties, 2D layered BP has been adopted to improve the UV responsivity of a photodetector.^[112]

Another important elemental group VI p-type semiconductor is Se, which possesses many excellent physical properties, such as low melting point (220 °C), high conductivity (8×10^4 S cm⁻¹), and relative high intrinsic carrier concentration (9.35×10^{16} cm⁻³).^[113] The bandgap of elemental Se is about 1.67 eV, indicating its potential for broadband photodetection. These specific properties make Se a very promising component for heterojunction UV-visible photodetectors with fascinating performance.^[114,115]

- 2) *Metal oxide*: p-type metal oxide semiconductors (such as CuO and NiO) have also been utilized to form p-n heterojunctions.^[116,117] A solution-processed p-n heterojunction photodiode is fabricated based on NiO and ternary Zn_{1-x}Mg_xO ($x = 0-0.1$). The fabricated visible-blind p-n junction photodetector demonstrates an excellent rectification ratio and displays good UV responsivity and high quantum efficiency.^[118]
- 3) *Metal chalcogenide*: Semiconducting metal chalcogenides mainly include group IIIA, IVA, and VA chalcogenides that have demonstrated their numerous intriguing characteristics and tremendous potential in photoelectric

detection.^[119,120] Especially, 2D TMDs with the generalized formula MX₂ (where M denotes a transition metal element and X denotes a chalcogen such as S, Se, or Te) possess certain bandgaps and are low-cost, earth-abundance, stable, and eco-friendly.^[121] The group VIB dichalcogenides (MoS₂,^[122] WS₂,^[123] MoSe₂,^[124] WSe₂,^[125] MoTe₂,^[126] WTe₂)^[127] with a moderate bandgap of 1–2 eV, are among the most representative TMDs.^[67] Except for materials mentioned above, researchers have also discovered and synthesized a number of novel TMDs, e.g., group IVB, VB, VIIB, and VIII dichalcogenides.^[128–130] These newcomers present various novel characteristics and compensate for the deficiencies of the conventional compounds.

These metal chalcogenides are regarded as hopeful components for heterojunctions, relying on the following advantages.^[131] First, the weak vdWs interaction and the absence of surface dangling bonds make heterostructures easier to construct by lowering the strict thermal and lattice-matching requirements. Second, some TMDs (e.g., 2H-MoS₂, 2H-WSe₂) show indirect-direct bandgap transition with decreasing layer numbers down to monolayer, which can be used to promote optoelectronic performance.

The heterojunctions containing TMDs have been widely adopted in UV photodetectors. 1D/1D heterostructures of ZnO/WS₂ core/shell nanowires are assembled in a single-nanowire photoresistive device. The photoelectric results show that the introduction of a few layers of WS₂ significantly enhances the photoresponse in UV range and drastically shortens the response time by almost two orders of magnitude, compared with the pure ZnO nanowire PD (Figure 3b).^[132]

A PtSe₂/GaN heterojunction is fabricated by in situ synthesis of vertically standing 2D PtSe₂ film on n-GaN substrate. The as-fabricated heterojunction device demonstrates excellent photo-response properties in deep-UV region and presents quick response to 266 nm pulse laser with a rise time of 172 ns.^[133] Another p-n diode is based on a stacked BP and rhenium disulfide (ReS₂) heterojunction. The heterojunction shows a clear gate-tunable rectifying behavior and displays a high photoresponsivity under UV illumination. Moreover, by adjusting the back-gate voltage, the photoresponse properties of this device can be tuned.^[112]

3. Heterojunction Integration for UV PDs

Heterojunction photodiodes are entitled with various materials and device architectures thanks to the abundant flexibility in material synthesis and device construction. The rapid development of semiconductors has effectively satisfied the material requirements, and plenty of studies have been reported to date with remarkable device performance. For one thing, the device performance of a heterojunction photodiode is partially determined by the individual material properties, such as carrier mobilities, doping density, energy band structure, and light absorption ability. For another thing, the energy band matching and the heterojunction interface may strongly influence the photoelectric properties.

The energy band matching plays an important role in heterojunctions. Compared to the homojunction, heterojunction offers extra situations besides the type II energy band matching owing to the different material bandgaps, and the potential barrier peak may also change the wavelength selectivity of a heterojunction photodiode. Therefore, high-efficiency single-color response,^[134] bi-color response,^[135] and bias-tunable color selectivity^[114] have been achieved in heterojunction photodiodes.

3.1. Lattice-Matched Heterojunction

However, the junction interface becomes a weak point for heterojunctions. Unlike that in homojunctions, severe lattice-mismatch often exists in heterojunctions and causes negative effects on device performance. Initially, the lattice-mismatch in-plane strain may deteriorate the contact quality of the two semiconductors, especially in crystallized materials. The weakened heterojunction with interface morphology defects such as wrappings and cracks can severely damage the electric properties of the heterostructure. What's more, the lattice mismatch introduces non-negligible surface states at the interface and influences the energy band structures, causing weaker junction barrier. Finally, the lattice mismatch itself may act as atomic interface defect. It can damage the uniformity of the built-in electric field and generates stronger Auger scattering effect to hinder the current collection and delay the response speed.^[136] Above all, the lattice mismatch is a considerable weak point of heterojunction, and special attention should be paid to the interface quality during the device construction.

Seeking lattice-matched materials may effectively solve the interface challenges resulting from lattice mismatch. As

presented in **Figure 4a**, naturally unstable Bi₂Se_{1.5}Te_{1.5} nanoplates are prepared on graphene substrate, where a high-performance photodetector is constructed.^[137] The interface structure is greatly optimized as lattice mismatch diminished, resulting in the increased material stability and the obvious performance enhancement. However, only a few heterojunction structures have been reported with acceptable lattice mismatch due to the variable crystal structures and lattice parameters of different semiconductors. Moreover, lattice-matched UV-sensitive heterojunctions are highly limited considering the additional bandgap requirements.

Some lattice-matched heterojunction devices based on moderate-bandgap materials can extend the response spectral to UV region and act as broadband UV-to-visible/IR photodetectors. For example, the lattice-matched Se/Si(111) heterojunctions are reported with broadband spectral response from UV to visible light, and the lattice matching contributes to a very fast response speed with improved photovoltaic properties (Figure 4b).^[22] However, the wavelength cutoff of these devices lies beyond the UV region and sets obstacles to selective UV detection or solar-blind UV detection. Wide-bandgap materials are preferred then.

Owing to the abovementioned material limitations, very few studies have been reported to achieve wide-bandgap lattice-matched heterojunctions, and we can only find GaN/ZnO,^[138] In_xAl_yGa_{1-x-y}N/GaN,^[139] and ZnO/Ga₂O₃^[140,141] to our best knowledge. GaN and ZnO both have wurtzite structures with similar lattice parameters (ZnO: *a* = 0.318 nm, *c* = 0.518 nm; GaN: *a* = 0.325 nm, *c* = 0.523 nm). High crystal quality p-GaN/n-ZnO bilayers are guaranteed using molecular beam epitaxy technique, and the lattice-matched heterojunction generates a clear rectifying effect with considerable bias-free UV photoresponse and a turn-on voltage of 3.7 V (Figure 5c). Similarly, large-bandgap In_xAl_yGa_{1-x-y}N quaternary alloy is reported to replace AlGaN to form heterojunction with GaN crystals, in which the lattice mismatch is kept small enough to avoid cracks and misfit dislocations. Apart from that, although the lattice mismatch of ZnO/Ga₂O₃ reaches about 5%, the interface energy is still effectively reduced to support a high-quality core-shell heterostructure, based on which novel UV photodetectors like piezo-phototronic effect modulated device^[141] and solar-blind avalanche photodiode^[140] are achieved.

Despite a few reported successful examples, the severe material limitation is still the biggest challenge of lattice-matched heterojunctions. Therefore, future studies should continue to focus on other lattice-matched materials. In addition, considering the highly limited material candidates, interface strategies like utilizing an interlayer are also worthy of consideration to reduce the negative effects of lattice mismatch.

3.2. Van der Waals Heterostructure

The prosperity of 2D crystals sheds light on their huge potential in optoelectronic devices. Many 2D crystals are entitled with excellent carrier mobility, and the vdWs force can support an excellent heterojunction interface regardless of the

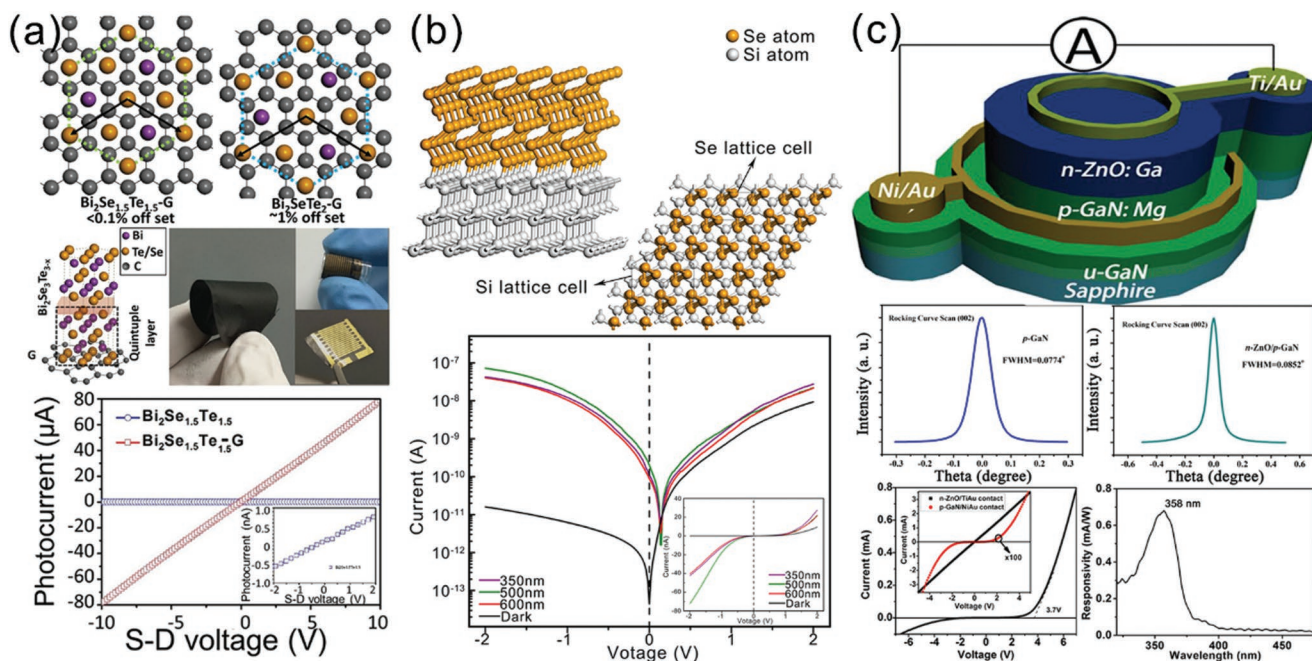


Figure 4. a) The reduced lattice mismatch and the enhanced device performance in Bi₂Se_{1.5}Te_{1.5}/graphene heterostructure photodiode and the I - V data of Bi₂Se_{1.5}Te_{1.5}/graphene and Bi₂Se_{1.5}Te_{1.5} device under illumination of 635 nm laser. Reproduced with permission.^[137] Copyright 2016, Wiley-VCH. b) The simulated lattice-matched lattice structure of Se/Si(111) interface and the I - V curves of fabricated photodiodes based on Se/Si(111) heterojunctions. Reproduced with permission.^[22] Copyright 2018, American Chemical Society. c) The high-quality lattice match in ZnO/GaN heterojunction and the solar-blind UV photoresponse of ZnO/GaN photodiodes with considerable rectification effect. Reproduced with permission.^[138] Copyright 2014, American Institute of Physics.

lattice-match condition thanks to the atomically sharp 2D structures.^[147] Therefore, numerous vdWs heterostructures have been reported based on a rich family of 2D crystals. However, only some of them are applicable for UV detection owing to the low device bandwidth. For example, 2D TMDs are one of the 2D crystal families, but their material bandgaps are typically limited to less than 2 eV, which is far below the UV border (3.1 eV). The low bandgaps reduce the UV photosensitivity and avoid the wavelength cutoff in the UV region. Wide-bandwidth vdWs heterostructures are still highly desired to achieve high-performance UV detection.

2D sandwich vdWs heterostructure, also called 2D Lego, in which different 2D crystals with various material properties are stacked together to finish the device construction, is a typical type of vdWs heterostructures.^[148] Metals or semimetals like graphene may act as electrode materials, and insulators like 2D hBN can serve as the dielectric layer. 2D semiconductor is used as the photosensitive layer here, and 2D semiconductors with larger material bandgaps are preferred in UV-sensitive 2D sandwiches. Compared to 2D TMDs, metal oxides and inorganic perovskite-type oxides with d0 transition metal atoms (Ti⁴⁺, Nb⁵⁺, Ta⁵⁺, W⁶⁺, etc.) have been reported to achieve large-bandgap 2D crystals in early studies.^[143] Figure 5a displays some of them. The monolayer Ti_{1- $\delta2$} on Si/SiO₂ substrate is reported with a thickness of merely 0.75 nm, and few-layer LaNb₂O₇ and Ca₂Nb₃O₁₀ nanosheets perform large bandgaps with selective UV absorption. Apart from the metal oxides, metal sulfides like HfS₂^[25] can also reach suitable large bandgaps in recent researches. However, many of them have not

been utilized in UV detectors because of the small size (several micrometers or less) caused by exfoliation process. Larger-size 2D crystals are usually produced by vapor-based growth so that the vdWs heterostructures can be formed directly on the epitaxial substrate or through a two-step transfer process. Few-layered 2D NiP₃ with a thickness of 3.2 nm have reached a lateral size of about 10 μm , and a high-performance solar-blind UV detector is constructed based on that with fast speed (≈ 5 ms) and ultralow dark current (10 fA).^[144] More impressively, ultrathin CuBr nanoflakes (0.91 nm) give an edge size of 45 μm and exhibits excellent solar-blind UV photoconductivity (Figure 5b).^[145] Although current reports have not focused on the vdWs heterostructures based on large-bandgap 2D crystals, these materials have the potential to form 2D sandwich heterojunction photodiodes.

Apart from pursuing large-bandgap 2D materials, forming 2D-XD hybrid vdWs heterostructures may make full use of the mature low-bandgap 2D crystals, in which low-bandgap 2D crystals like 2D TMDs or graphene are composited with non-2D wide-bandgap semiconductors. As mentioned in last section, the low-bandgap 2D crystals mainly serve as carrier blocking layer or current collector in the UV region and the composited semiconductors absorb the incident UV light. The hybrid vdWs heterostructures combine UV photosensitivity and high carrier mobility, and a promoted UV detection (usually broadband spectral response) is achieved. For example, ZnO QDs are printed on graphene and generated a 2D-0D hybrid vdWs heterostructure with ultrasensitive detection of UV light,^[146] and other nanocrystals like FeS₂-PbS^[149]

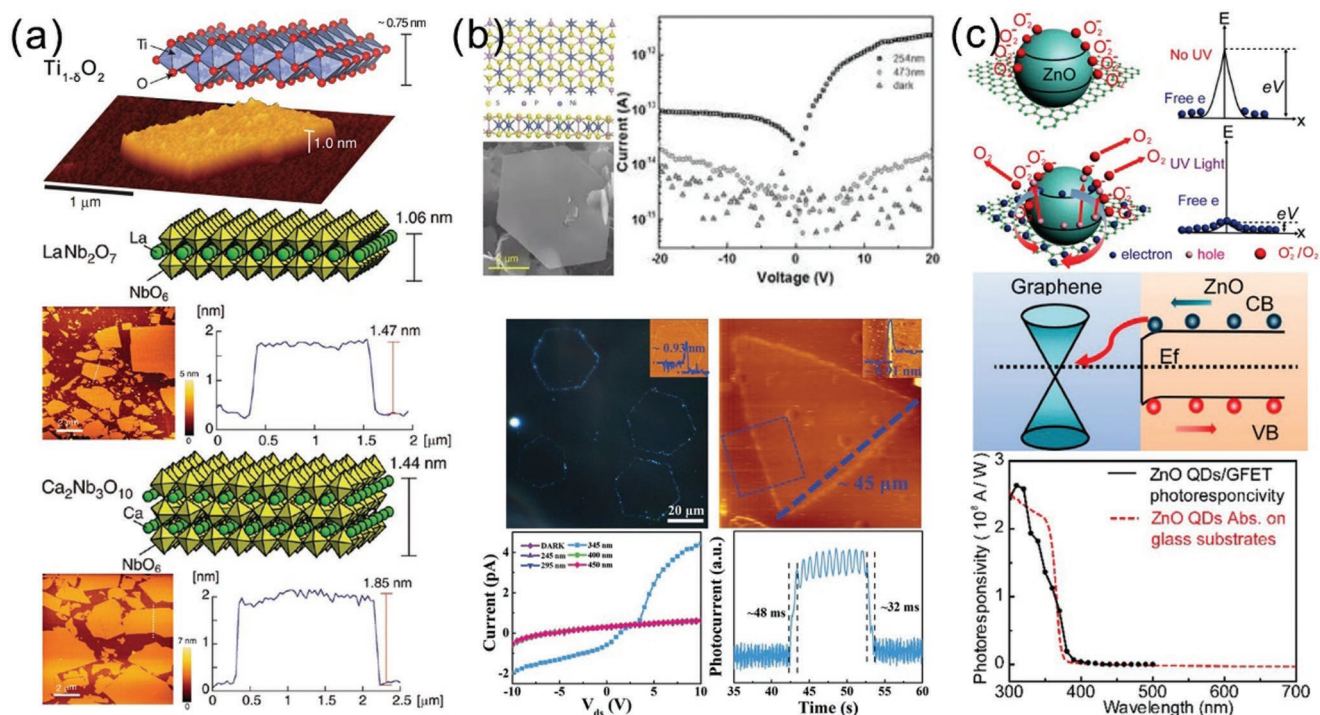


Figure 5. a) The AFM data and the crystal structures of some wide-bandgap 2D semiconductors which have the potential to be used for UV detection, including few-layer $\text{Ti}_{1-x}\text{O}_2$ (top),^[143] LaNb_2O_7 (middle),^[142] and $\text{Ca}_2\text{Nb}_3\text{O}_{10}$ (bottom).^[142] Reproduced with permission.^[142] Copyright 2010, American Chemical Society and reproduced with permission.^[143] Copyright 2012, Wiley-VCH. b) Morphologies and device performance of UV detectors based on large-size wide-bandgap 2D crystals (top: NiPS_3 ,^[144] bottom: CuBr).^[145] Reproduced with permission.^[144] Copyright 2017, Wiley-VCH and reproduced with permission.^[145] Copyright 2019, Wiley-VCH. c) 2D-0D Hybrid vdWs heterostructure device based on ZnO QD/graphene and its selective UV response according to the spectral performance. Reproduced with permission.^[146] Copyright 2017, American Chemical Society.

and FeS_2 ^[150] are utilized to similarly strengthen the light absorption in other reports. Apart from the 2D-0D hybrid vdWs structures, 2D-0D hybrid structures based on bulk semiconductor crystals are also reported. Bulk GaAs can be used to enhance the short-wavelength absorption and constructed a heterojunction photodiode with graphene.^[26] Their device exhibits a self-powered broadband photoresponse from 325 to 980 nm and the device performance is further improved by sputtering Ag particles.

In general, the UV-sensitive vdWs junction has huge advantages in ultrafast photoresponse and it is in a rapid development now. More and more researchers become interested in the fabrication as well as the photoelectric properties of large-bandgap 2D crystals, but studies on the device constructions are still insufficient. In addition, although there is no need to worry about the lattice mismatching in vdWs structures, interface defects may still exist in nonepitaxial heterostructures owing to the residual solution or the environmental contaminants. Encapsulation methods are also considerable to stabilize the device performance under air exposure.

3.3. Other Heterojunctions

Heterojunctions used to be defined as junctions combining semiconductors with closely matched lattice and different bandgap

energies.^[21] They tend to form strong chemical bonds and strongly depend on lattice similarity and similar electronic properties, which reduces the possibilities of integrating different materials for better behaviors. Since the blossoming of nanoscience and the exploration of diverse materials of different dimensions, the previous definition is not suitable for research nowadays.^[24]

As stated before, lattice matching can suppress capturing photogenerated carriers and enhance the separation as well as collection efficiency of photogenerated carriers.^[151] Research on 2D materials leads the attention to vdWs integration where different materials are assembled together with weak vdWs interactions.^[24] Although these heterojunctions give excellent interface properties with enhanced device performance, they also suffer severe limitation of finite material candidates and poor surface roughness that is not able to create vdWs integrations. Other heterostructures are worthy of consideration to construct goodish devices, which is fortunately available for almost all semiconductor materials. Therefore, we here expand the scope of a heterojunction and take a general look at heterostructures, in which materials of different dimensions can be integrated not only by chemical epitaxial growth or physical vapor deposition, but also through a lot of simple methods, such as drop-casting, spin-coating, and dip-coating.

This part mainly focuses on those heterojunctions/heterostructures apart from lattice matching and vdWs integration, most of which are semiconductor–semiconductor junctions^[108,114,115,151] and semiconductor–conductive materials

junctions.^[19,20,152] The basic function of a heterojunction is to create built-in electrical fields near the interfaces and effectively separate photogenerated carriers.^[114,115,153] A typical example is the heterojunction between BiOCl nanosheets and TiO₂ nanotubes (NTs).^[98] The junction is prepared by simple impregnation methods, and the performance is comprehensively improved because of built-in electrical field. The response speed is improved because depletion region stops the carriers transport when light stimulation is off, thus leads to extremely low dark current. It is interesting that the amount and orientation of BiOCl nanosheets have great impact on the performance. Only proper growth of BiOCl (six spin-coating cycles of BiOCl on TiO₂) can result in synergistic effect of p-n heterojunction and the self-induced internal electric field.

Many heterojunctions are integrated just by simple methods such as sputtering, direct transferring, and spin-coating.^[13,29,153–159] It is a much more flexible way to combine various materials of different dimensions. Here, we put an example of perovskite QDs decorated TiO₂ NTs synthesized by simple spin-coating methods. In general, perovskite QDs would suffer from UV photobleaching and poor stability. It is worth noting that through the weak binding between perovskite and TiO₂, the stability is improved and the device can survive the 72 h stability test in wet air. In this article,^[7] the reason TiO₂ NTs outperformed TiO₂ NWs lies in the special tubular structure, which causes a much thicker depletion layer leading to higher photocurrent.

Heterojunctions based on organic semiconductors also have achieved great progress in recent years. Considering that the requirements of lattice-matching junction and van der Waals integration are not quite suitable for organic materials, they are often assembled via simple fabrication process. A donor-acceptor-type heterojunction is constructed in such way by combining electron-deficient isoindigo (II) and electron-rich thienoisindigo.^[160] Isoindigo π - π^* transitions contribute to the UV-visible absorption. Through 2D covalent-organic framework (COF) integration with soluble fullerene derivative (PC₇₁BM), the device realizes nearly complete inversion of spectral sensitivity between blue and red light as well as green and NIR range for the first time. PC₇₁BM can also be used in organic photodiodes to break the compromise between responsivity and response speed.^[161]

Due to relatively accommodative requirements to build such kind of heterojunctions, naturally researchers have more freedom to realize some complex structures. In a Ga₂O₃-based device (Figure 6a), it is apparent that the strategy of using two back-to-back junctions formed a pronounced rectifying effect, and the device exhibits good selectivity with peak sensitivity at ≈ 220 nm.^[20] The junctions are assembled via simple multilayer graphene transfer. However, the response speed is very slow (rise/fall time = 94.83 s/219.19 s), in exchange for high responsivity and EQE (responsivity = 39.3 A W⁻¹, EQE = 1.96 $\times 10^4\%$ at 20 V).

For heterojunctions with distorted lattice, it is a smart strategy to build an upper heterojunction to create dual built-in electrical fields. p-type organic poly(3,4-ethylenedioxythiophene):polystyrene sulfonate (PEDOT:PSS) with high transparency is insensitive to interface defects, thus is appropriate for constructing an upper heterojunction (Figure 6b).^[151] During

the formation of Ga₂O₃/p-Si heterojunction, the barrier construction would be hindered by interface oxygen vacancies and carriers could not be collected. But with the help of Schottky barrier between PEDOT:PSS and Ga₂O₃, carrier separation is so greatly enhanced under the force of built-in electrical field, that EQE reaches 15% without any external power supply. The photovoltaic device responds quickly to deep ultraviolet (240 nm) at the speed of 60 ms (rise time) and 88 ms (decay time).

New type junctions can also prevent high recombination of photogenerated carriers in a more efficient way. An atomic layer deposition (ALD) alumina inversion layer is added to further minimize surface recombination.^[162] What's more, it reduces dopant-induced recombination as well. This photodiode consisting of black silicon and alumina exhibits a wide response spectral (250–950 nm) without external power supply, and the highest EQE dramatically reaches 96% for the whole response range. The strategy greatly increases the density of effective charges.

As it is possible to directly combine different materials for better photodetection performance, combining other electronic effect seems easy to realize. ZnO is a common UV-sensitive material with pyroelectric effect. In a report, the pyro-photoelectric three-way coupling effect makes it possible to take strong control over photogenerated carrier transport.^[163] The Si/ZnO p-n junction is prepared by sputtering seed layer and hydrothermal methods. Charge carriers transport is greatly influenced by the pyro-polarization owing to the light-induced transient temperature change when UV is on/off, thus the response speed and responsivity are significantly improved.

Piezoelectric polarization charges can also be produced when applying external strain to ZnO as shown in Figure 6c.^[152] Pyropolarization and piezopolarization can be coupled in a ZnO-based heterojunction to realize self-powered UV photodetectors. A simple PEDOT:PSS/ZnO heterojunction is assembled through spin-coating methods. The pyroelectric mechanism is similar to p-Si/ZnO p-n junction.^[163] In this way, external strain is used to further control pyropolarization and photovoltaic effect from p-n junction. Thanks to the four-way coupling, the photocurrent dramatically increases by 600% with fast response speed.

Ferroelectric materials are often used in UV detection for regulating the distribution of photogenerated carriers, for example, the combination of UV-response ZnO and self-polarized BaTiO₃.^[164] The ferroelectric localized field introduced by common ferroelectric films depletes those defect/trap-induced carriers and decreases dark current.^[165–167] In a heterojunction, the ferroelectric field can modulate the junction energy band so that the transport and separation of photogenerated carriers are efficiently promoted. The heterojunction between ferroelectric V-doped ZnO nanosheets and p-Si exhibits an increased responsivity and fast response speed, which indicates a promising route to design high-performance heterojunction UV PDs.^[168]

Heterojunctions that efficiently reduce charge recombination and enhance charge separation are also a very important part of PEC photodetectors to modify photoanodes.^[169] For instance, the TiO₂/SnO₂ branched heterojunction that works as a PEC type photodetector presents a self-powered property with high

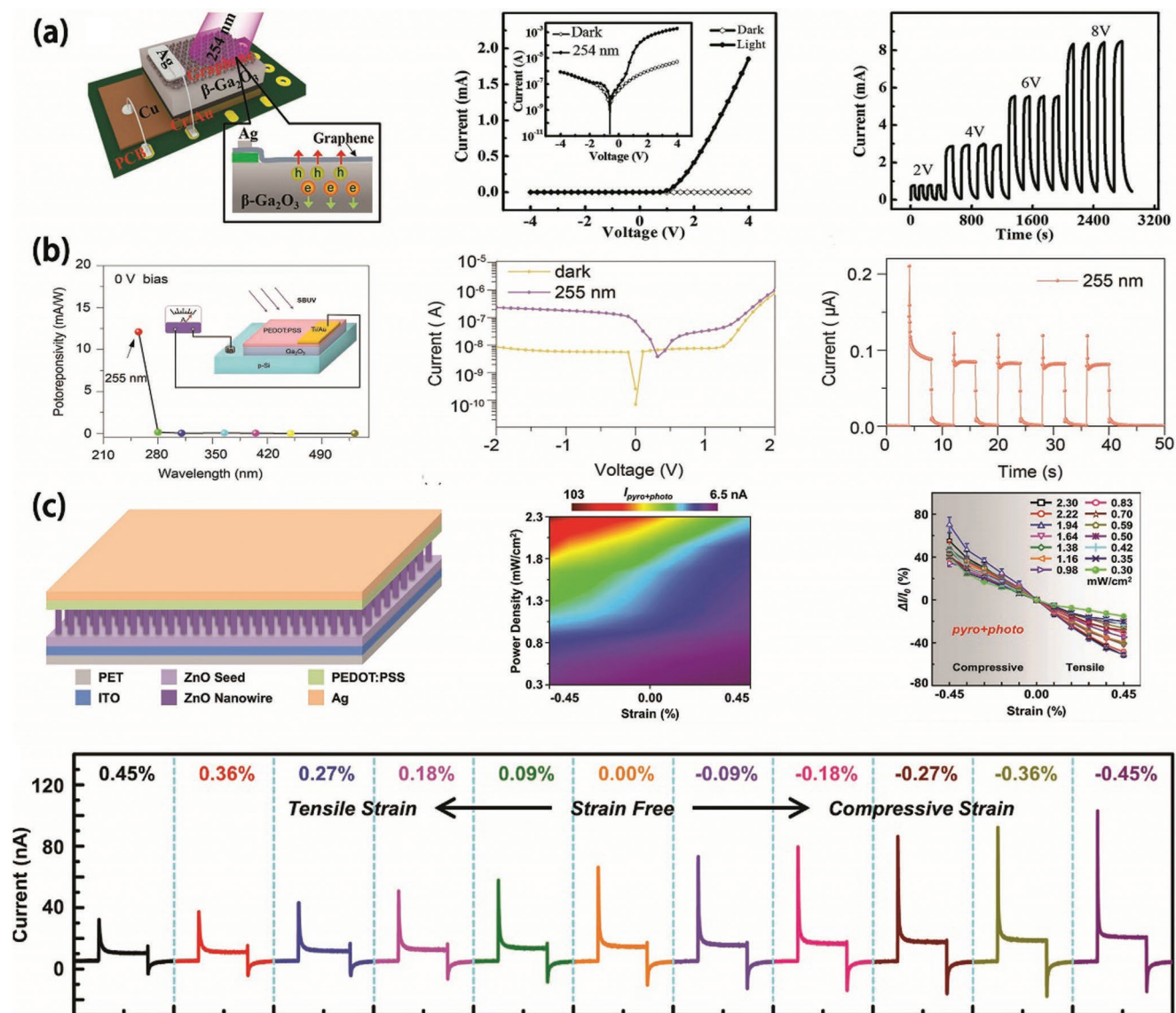


Figure 6. a) Schematic diagram, I - V curves in dark and under 254 nm irradiation and current at 2, 4, 6, and 8 V of multilayer graphene/ β - Ga_2O_3 deep UV PD. Reproduced with permission.^[20] Copyright 2016, Wiley-VCH. b) Spectral response at 0 V bias, test diagram, I - V characteristic curve in dark and under 255 nm illumination, and time-dependent photocurrent of PEDOT:PSS/ Ga_2O_3 /p-type Si device. Reproduced with permission.^[151] Copyright 2019, Wiley-VCH. c) Schematic diagram, 2D mapping of the pyro-phototronic and piezo-phototronic current, relative change of $I_{\text{pyro+photo}}$, $\Delta I/I_0$ of PEDOT:PSS/ZnO heterojunction. Reproduced with permission.^[152] Copyright 2017, Wiley-VCH.

responsivity of 0.6 A W^{-1} under UV illumination.^[170] The heterostructure of TiO_2/ZnO also suppresses charge recombination due to well-designed type-II energy band alignment.^[171] These works provide an instructive strategy to build PEC type heterojunction UV photodetectors.

We review different heterojunctions in this section and classify them into different kinds according to junction interactions: lattice-matched heterojunctions, vdWs heterostructures, and other heterojunctions. And we list some typical representatives in Table 1 trying to follow the tracks of recent research. Each of the three kinds has unique requirements for materials and leads to different properties. It is smart to choose proper integration methods before constructing a heterojunction/heterostructure for enhanced photodetection.

4. Heterojunction UV PD Applications

Since heterojunction UV photodetectors are receiving increasing attention for its excellent properties, some future applications are also investigated. Here, we mainly introduce some practical photodetectors that are the basis of future wearable or implantable smart devices.

MAPbI_3 QDs decorated TiO_2 NTs are promising for flexible PDs when constructed on mica substrates through simple spin-coating methods (Figure 7a).^[7] On rigid substrates the heterojunction represents excellent photodetection ability, and when substrates are changed for mica the performance shows good stability. The device shows high flexibility with stable optoelectronics performance, as well as high transparency. The

Table 1. Different kinds of heterojunction UV PDs.

Heterostructure type	Active materials	Wavelength [nm]	Bias [V]	Responsivity [mA W^{-1}]	D^* [Jones]	Response speed		Reference
						Rise time	Fall time	
Lattice matching	Se/n-Si	350–600	–2	–	–	–	–	[22]
	GaN/ZnO	358	0	0.68	–	–	–	[138]
	ZnO/Ga ₂ O ₃	251	0	9.7	6.29×10^{12}	100 μs	900 μs	[140]
	ZnO/Ga ₂ O ₃	268	–3	–	–	–	–	[141]
van der Waals	NiPS ₃	254	10	126	1.22×10^{12}	3.2 ms	≈ 17.5 ms	[144]
	CuBr	345	10	3.17×10^3	1.4×10^{11}	32 ms	48 ms	[145]
	ZnO QDs/graphene	340	10	9.9×10^{11}	$> 1 \times 10^{14}$	5 s	85.1 s	[146]
	V-HfS ₂	405	1	–	–	24 ms	24 ms	[25]
	FeS ₂ -PbS/graphene	340	0.1	1.78×10^9	6.46×10^{11}	–	–	[149]
	FeS ₂ /graphene	340	0.1	1.78×10^9	8.76×10^{11}	0.6 s	0.6 s	[150]
	Graphene/GaAs	325	0	186	2.63×10^{13}	–	–	[26]
Others	PEDOT:PSS/Ga ₂ O ₃ /p-Si	240	0	0.029×10^3	–	60 ms	88 ms	[151]
	Graphene- β -Ga ₂ O ₃	254	20	39.3×10^3	5.92×10^{13}	94.83 s (4 V)	219.19 s (4 V)	[20]
	MAPbI ₃ /TiO ₂	350	1	1.3×10^3	2.5×10^{12}	2 s	1 s	[7]
	Si/ZnO	325	–0.04	13	–	19 μs	22 μs	[163]
	PEDOT:PSS/ZnO	325	0	3.5	7.5×10^9	5.8 ms	7.3 ms	[152]
	BiOCl/TiO ₂	350	–5	41.94×10^3	1.41×10^{14}	12.9 s	0.81 s	[98]
	GD:ZnO/ZnO	365	10	1260×10^3	–	6.1 s	2.1 s	[108]
	CuZnS/TiO ₂	350	3	6.4×10^5	–	–	–	[134]
	ZnO/PVK	325	0.2	30	–	1.5 s	6 s	[172]
	TiO ₂ /MAPbI ₃	350	1	1300	2.5×10^{12}	2 s	1 s	[7]
	ZnO/Zn ₂ SnO ₄	300	1	–	9.0×10^{17}	47 ms	47 ms	[173]

photocurrent stays almost unchanged when bending at 0°, 45°, 90°, 180° and keeps stable after 200 cycles when bending to 90°.

A solar-blind photodetector is constructed on a graphene–diamond heterojunction.^[158] The microcrystalline diamond can be easily peeled off from Si substrates because of internal residual stress resulting from lattice mismatching. Thus, applying the diamond thin film to tapes would complete a flexible PD. Monolayer graphene is transferred to the surface of diamond/Au electrode/tape film through wet-transfer method. This flexible junction shows high responsivity under stimulation of 220 nm illumination because of the photogain resulting from the defects at graphene/diamond interface.

Fiber photodetectors are a typical kind of flexible optoelectronics. As shown in Figure 7b, a p-n junction based self-powered fiber photodetector is prepared and shows a high responsivity (9.96 mA W^{-1}).^[172] The built-in electric field between ZnO and polyvinylcarbazole (PVK) is used to separate photogenerated charge carriers. This optoelectric fiber can be woven into a web and bent at 90°. In Figure 7c, another fiber PD is based on the p-n junction between p-CuZnS and n-TiO₂.^[134] It is obvious that the PD shows typical rectifying characteristics and owns an ultrahigh responsivity (640 A W^{-1} at 3 V) toward UV light. Thanks to the high photocurrent ($\approx \text{mA}$), the device can be integrated with commercial electronics and forms a real-time UV monitoring system, which can send UV intensity to phones and can be used as a wearable device. The excellent

performance is mainly attributed to conformal coating of p-CuZnS on TiO₂ and the 360° collection of photocarriers.

Due to the small volume of a fiber, it seems easier for fiber PDs to achieve large-scale integration. Human hair can act as the core for supporting a fiber PD.^[96] As seen from Figure 8a, simple sputtering and hydrothermal strategies are in turn applied to form the Al-doped ZnO/ZnO nanorods layer on a hair substrate. PVK and PEDOT:PSS are used to form p-n junction and transport holes, respectively. Under different bending states, the heterostructure exhibits good stability and the photocurrent only reveals a slight fluctuation. Based on this flexible fiber photodetector, photon-triggered logic gates and a UV image sensor are fabricated. The logic gates are constructed by integrating several hair-based photodetectors into circuits. This system can be used as phototriggered AND, OR, and NAND logic gates. Researchers also use seven heterojunctions to form a conceptual image sensor showing clear numbers.

A more complex UV image sensor is fabricated (Figure 8b).^[173] The heterojunction consisting of ZnO QDs decorated Zn₂SnO₄ nanowires is assembled via a solvothermal process. Through band engineering, the ZnO QDs effectively help to separate electron–hole pairs and lead to high UV light photoresponse. The photoconductive gain reaches 1.1×10^7 and the speed is quite fast (47 ms). The flexible PD is fabricated on PET, and the performance

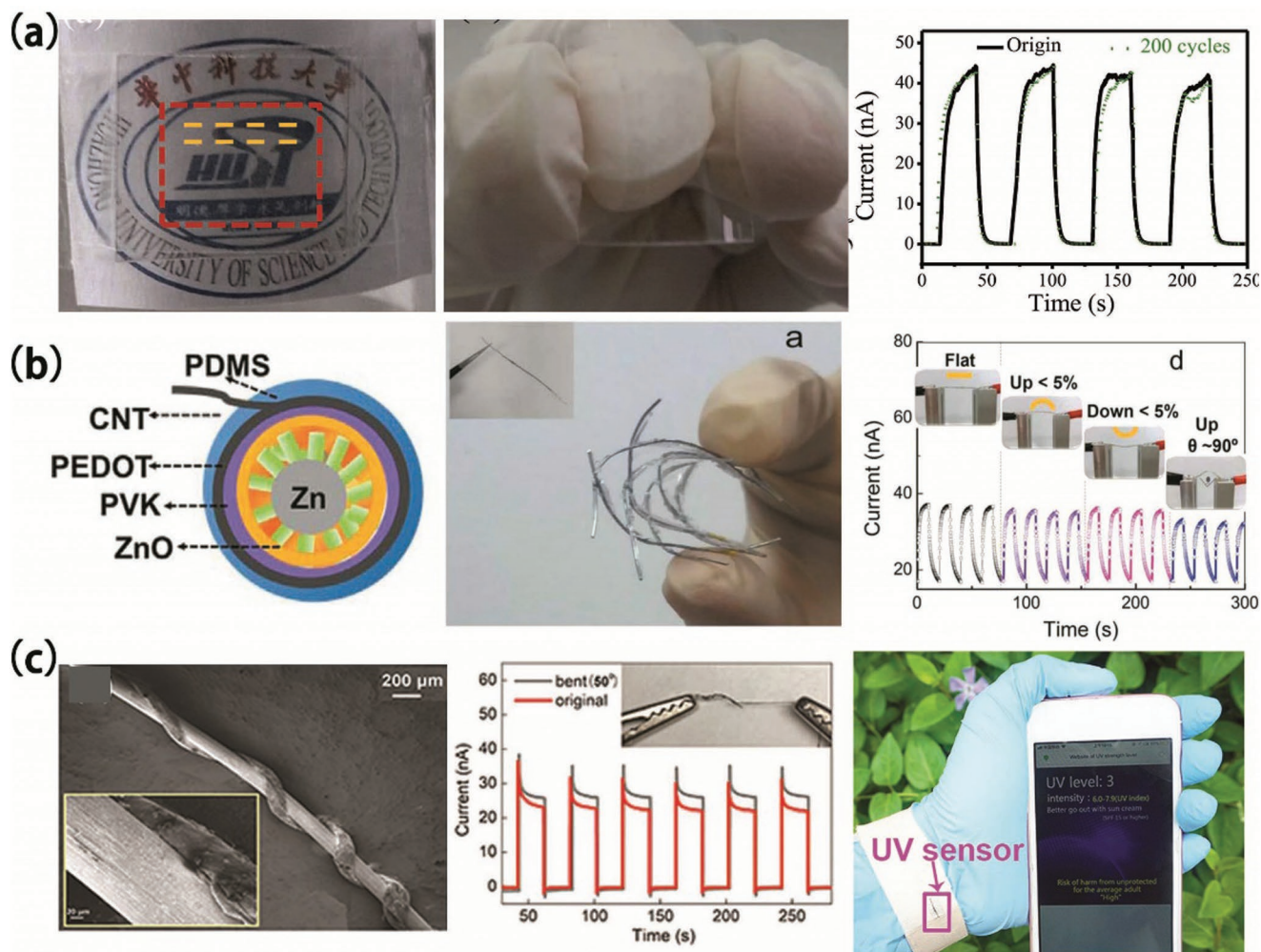


Figure 7. a) Optical images and $I-t$ curves before and after bending of the flexible and transparent heterojunction based on MAPbI₃ QDs decorated TiO₂ NTs. Reproduced with permission.^[7] Copyright 2017, Wiley-VCH. b) Schematic representation, optical images, and $I-t$ curves at different bending states of ZnO/PVK PD. Reproduced with permission.^[172] Copyright 2016, Elsevier Ltd. c) SEM image, on-off switching tests at different states and applications of CuZnS/TiO₂ PD. Reproduced with permission.^[134] Copyright 2018, Wiley-VCH.

remains almost unchanged after 2000 bending cycles at 150°. The image sensor is constructed using 10 × 10 heterojunction arrays, indicating that the device has the potential for future application.

In this part, we briefly introduce several applications of heterojunction UV photodetectors about flexible and wearable electronics, image sensors, and logic circuits. Ultraviolet is a very important part of light spectrum, and it will play a more essential role in medical treatment, military development, and daily life once we are confident enough on the technique maturity. With the unceasing progress of material synthesis and device assembly technologies, more gripping applications of UV photodetectors can be expected.

5. Summary and Outlook

This article provides a summary of heterojunction UV PDs in recent years. The photoelectric performance of a heterojunction

photodetector is determined by the composition and the way of integration.^[174–176] We have summarized some new developed building blocks applied in heterojunction/heterostructure UV PDs. They are separated into two parts: half part of a heterojunction is semiconductors with light response, while the other half is functionalized with specific effects. Their physical and chemical properties are concisely and comprehensively introduced. Then a discussion regarding different kinds of heterojunction/heterostructure UV PDs has been given. Lattice-matched heterojunctions without interface defects and interface surface states show greatly improved performance, but only a few combinations of semiconductors can meet the strict requirements. VdWs integrations are free from one-by-one chemical bonds and have huge potential in UV photodetection, yet there is still a long way to go considering their synthesis and stability in air. Other heterojunctions with rough interfaces seem much easier to integrate, while they inevitably suffer from defects and surface states at the interface. After that, we have also presented some specific applications of heterojunctions/heterostructures

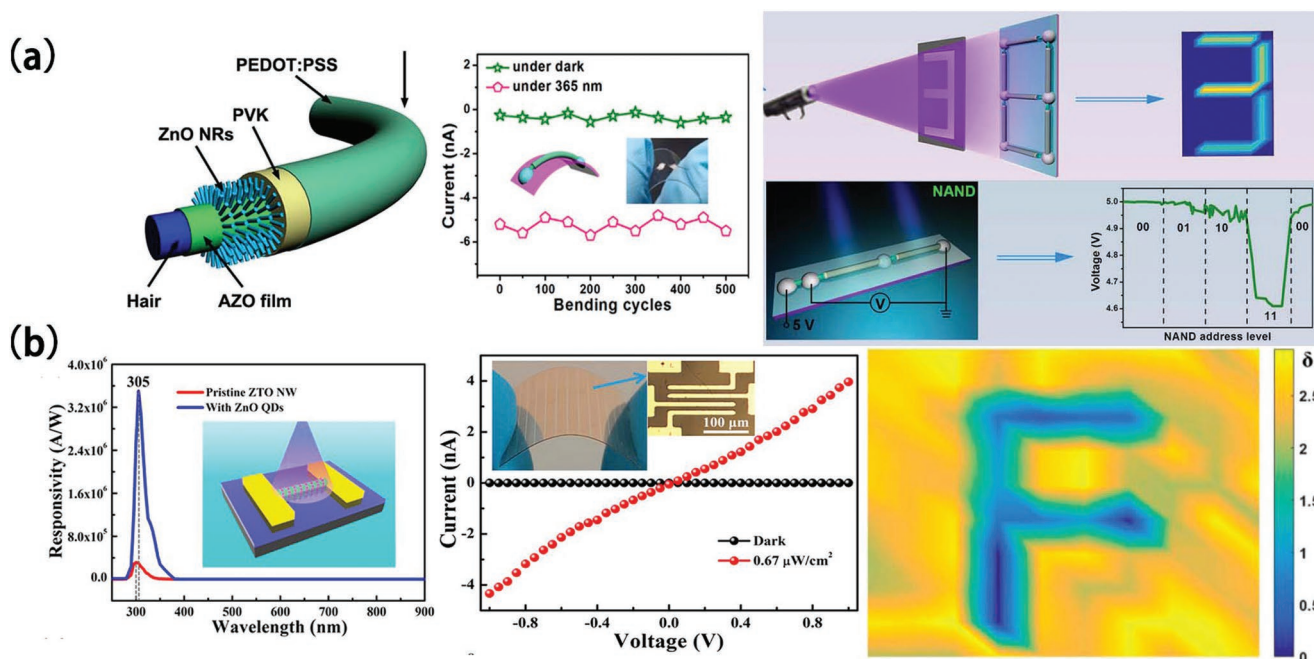


Figure 8. a) Schematic diagram, photocurrent before and after bending, and applications of Al:ZnO/ZnO/PVK/PEDOT:PSS PD. Reproduced with permission.^[96] Copyright 2019, American Chemical Society. b) Spectral responsivity, I - V curves, and output images of letters of flexible ZnO/Zn₂SnO₄ PD. Reproduced with permission.^[173] Copyright 2017, American Chemical Society.

on flexible photodetectors and image sensors. In the end, we put forward several issues worthy of paying attention to.

It is undoubted that 2D materials are the most favored materials for present UV PDs research. 2D layered semiconductors that span chalcogenides, halides, nitrides, and other composites show strong interaction with incident light. Moreover, they are provided with high carrier mobility, significant quantum confinement effect, and satisfactory photon absorption as well as electron-hole generation efficiency. Additionally, 2D nonlayered materials filled with surface dangling bonds endow their surfaces with high chemical activity, which can be necessary complement to 2D layered materials. Attention should be paid to adjusting the dimension and the conducting of intercalation, which can modify the electronic and optoelectronic properties and leads to promotion of related devices. It is worth noting that because of their high transparency and good mechanical flexibility, the atomic-thick 2D layered semiconductors provide the possibilities for flexible, wearable, or portable electronics. Last but not least, despite pursuing the extreme of individual device, to enhance the stability, scalability, and processability of 2D materials-based photodetectors should carry the same weight.

As for heterojunction integration, vdWs integrations are assembled by weak interactions and provide an alternative bond-free integration strategy, which realizes excellent performance via multiple combination of diverse materials regardless of lattice and processing compatibility. However, considering the uniformity, surface contamination, and transferring process that largely rely on manual operation proficiency, it is still challenging to realize scalable production of reliable and stable vdWs heterostructure device. Moreover, high-performance semiconductors are not limited within two dimensions. Developing

vdWs integration of various dimensions with atomically clean and electronically sharp interfaces is also a big challenge.

The challenges for practical heterojunction UV PDs are the reliability and the integration. In accordance with our review, most UV PDs are applied in flexible devices. Other materials with intrinsic rigidity and brittleness are difficult to bend and some interactions between materials are not strong enough to bear the stress, such as vdWs assembling. To realize flexibility, UV response heterojunctions are usually constructed on flexible planar or fiber substrates, which encounters a latent problem of holding substrates and materials together. In addition, large-scale integration of heterojunction UV photodetectors seems beyond realization, unless the technology grows mature to produce quite reliable heterojunctions. And these need endless efforts from fabrication of heterojunction building blocks to designing of heterojunction architecture, especially dealing with interface conditions carefully.

As presented, more efforts should be made to take full advantage of heterojunctions for efficient photodetection. Generally, it is still a great strategy to integrate heterojunction UV PDs with carefully selected building blocks and well-aligned energy bands for suppressing dark current, improving response speed, and gaining high quantum efficiency.

Acknowledgements

J.X.C., W.X.O., and W.Y. contributed equally to this work. The work was supported by National Key R&D Program of China (Nos. 2017YFA0204600 and 2018YFA0703700), National Natural Science Foundation of China (Nos. 51872050 and 11674061), the China Postdoctoral Science Foundation (Nos. 2018M640338 and 2019T120299), Science and Technology Commission of Shanghai

Municipality (Nos. 19520744300, 18520710800, and 18520744600), and the startup fund of City University of Hong Kong.

Conflict of Interest

The authors declare no conflict of interest.

Keywords

heterojunctions, lattice-matched heterojunctions, semiconductors, ultraviolet photodetectors, van der Waals heterostructures

Received: November 27, 2019

Revised: December 18, 2019

Published online: February 14, 2020

- [1] H. Y. Chen, K. Liu, L. Hu, A. A. Al-Ghamdi, X. S. Fang, *Mater. Today* **2015**, *18*, 493.
- [2] F. Teng, K. Hu, W. Ouyang, X. S. Fang, *Adv. Mater.* **2018**, *30*, 1706262.
- [3] S. J. A. Moniz, S. A. Shevlin, D. J. Martin, Z.-X. Guo, J. Tang, *Energy Environ. Sci.* **2015**, *8*, 731.
- [4] A. M. Al-Amri, B. Cheng, J.-H. He, *IEEE Trans. Nanotechnol.* **2019**, *18*, 1.
- [5] G. Konstantatos, E. H. Sargent, *Nat. Nanotechnol.* **2010**, *5*, 391.
- [6] C. Xie, C.-K. Liu, H.-L. Loi, F. Yan, *Adv. Funct. Mater.* **2019**, *29*, 1903907.
- [7] Z. Zheng, F. Zhuge, Y. Wang, J. Zhang, L. Gan, X. Zhou, H. Li, T. Zhai, *Adv. Funct. Mater.* **2017**, *27*, 1703115.
- [8] Y. Zhan, Y. Wang, Q. Cheng, C. Li, K. Li, H. Li, J. Peng, B. Lu, Y. Wang, Y. Song, L. Jiang, M. Li, *Angew. Chem., Int. Ed.* **2019**, *58*, 1.
- [9] Y. Wang, F. Yang, X. Li, F. Ru, P. Liu, L. Wang, W. Ji, J. Xia, X. Meng, *Adv. Funct. Mater.* **2019**, *29*, 1904913.
- [10] C.-H. Lin, B. Cheng, T.-Y. Li, J. R. D. Retamal, T.-C. Wei, H.-C. Fu, X. S. Fang, J.-H. He, *ACS Nano* **2018**, *13*, 1168.
- [11] S. Li, Y. Zhang, W. Yang, H. Liu, X. S. Fang, *Adv. Mater.* **2020**, *32*, 1905443.
- [12] A. M. Alamri, S. Leung, M. Vaseem, A. Shamim, J.-H. He, *IEEE Trans. Electron Devices* **2019**, *66*, 2657.
- [13] S. Abbas, M. Kumar, D.-W. Kim, J. Kim, *Small* **2019**, *15*, 1804346.
- [14] S. Cai, X. J. Xu, W. Yang, J. X. Chen, X. S. Fang, *Adv. Mater.* **2019**, *31*, 1808138.
- [15] Z. Zhang, P. Lin, Q. Liao, Z. Kang, H. Si, Y. Zhang, *Adv. Mater.* **2019**, *31*, 1806411.
- [16] N. Huo, G. Konstantatos, *Adv. Mater.* **2018**, *30*, 1801164.
- [17] K. Yan, Z. Wei, T. Zhang, X. Zheng, M. Long, Z. Chen, W. Xie, T. Zhang, Y. Zhao, J. Xu, Y. Chai, S. Yang, *Adv. Funct. Mater.* **2016**, *26*, 8545.
- [18] H. Tan, A. Jain, O. Voznyy, X. Lan, F. P. G. d. Arquer, J. Z. Fan, R. Quintero-Bermudez, M. Yuan, B. Zhang, Y. Zhao, F. Fan, P. Li, L. N. Quan, Y. Zhao, Z.-H. Lu, Z. Yang, S. Hoogland, E. H. Sargent, *Science* **2017**, *355*, 722.
- [19] R. Lin, W. Zheng, D. Zhang, Z. Zhang, Q. Liao, L. Yang, F. Huang, *ACS Appl. Mater. Interfaces* **2018**, *10*, 22419.
- [20] W. Y. Kong, G. A. Wu, K. Y. Wang, T. F. Zhang, Y. F. Zou, D. D. Wang, L. B. Luo, *Adv. Mater.* **2016**, *28*, 10725.
- [21] H. Kressel, *Annu. Rev. Mater. Sci.* **1980**, *10*, 287.
- [22] W. Yang, K. Hu, F. Teng, J. Weng, Y. Zhang, X. S. Fang, *Nano Lett.* **2018**, *18*, 4697.
- [23] S.-J. Liang, B. Cheng, X. Cui, F. Miao, *Adv. Mater.* **2019**, 1903800.
- [24] Y. Liu, Y. Huang, X. Duan, *Nature* **2019**, 567, 323.
- [25] B. Zheng, Y. Chen, Z. Wang, F. Qi, Z. Huang, X. Hao, P. Li, W. Zhang, Y. Li, *2D Mater.* **2016**, *3*, 035024.
- [26] Y. Lu, S. Feng, Z. Wu, Y. Gao, J. Yang, Y. Zhang, Z. Hao, J. Li, E. Li, H. Chen, S. Lin, *Nano Energy* **2018**, *47*, 140.
- [27] A. A. Chaaya, M. Bechelany, S. Balme, P. Miele, *J. Mater. Chem. A* **2014**, *2*, 20650.
- [28] W. Tian, H. Lu, L. Li, *Nano Res.* **2015**, *8*, 382.
- [29] W. X. Ouyang, F. Teng, M. Jiang, X. S. Fang, *Small* **2017**, *13*, 1702177.
- [30] X. S. Fang, L. F. Hu, K. F. Huo, B. Gao, L. J. Zhao, M. Y. Liao, P. K. Chu, Y. Bando, D. Golberg, *Adv. Funct. Mater.* **2011**, *21*, 3907.
- [31] W. X. Ouyang, F. Teng, J.-H. He, X. S. Fang, *Adv. Funct. Mater.* **2019**, *29*, 1807672.
- [32] D. Gedamu, I. Paulowicz, S. Kaps, O. Lupan, S. Wille, G. Haidarschin, Y. K. Mishra, R. Adelung, *Adv. Mater.* **2014**, *26*, 1541.
- [33] K. M. Chahrour, F. K. Yam, R. Abdalrheem, *Mater. Lett.* **2019**, 248, 161.
- [34] Y. Li, W. Huang, H. Liu, J. Wang, L. Tian, S. Zhang, *J. Nanopart. Res.* **2018**, *20*, 334.
- [35] Y. Dong, S. Wang, Y. Zou, S. Liu, Z. Zhu, J. Li, D. Ju, J. Chen, K. Zhang, X. Liu, H. Zeng, *Adv. Mater. Technol.* **2018**, *3*, 1800085.
- [36] S.-H. Tsai, S. Basu, C.-Y. Huang, L.-C. Hsu, Y.-G. Lin, R.-H. Horng, *Sci. Rep.* **2018**, *8*, 14056.
- [37] X. Han, S. Feng, Y. Zhao, L. Li, Z. Zhan, Z. Tao, Y. Fan, W. Lu, W. Zuo, D. Fu, *RSC Adv.* **2019**, *9*, 1394.
- [38] C. Yan, N. Singh, P. S. Lee, *Appl. Phys. Lett.* **2010**, *96*, 053108.
- [39] Z. Zhipeng, H. von Wenckstern, M. Grundmann, *IEEE J. Sel. Top. Quantum Electron.* **2014**, *20*, 106.
- [40] M. Rui, X. Li, L. Gan, T. Zhai, H. Zeng, *Adv. Funct. Mater.* **2016**, *26*, 5051.
- [41] X. J. Xu, S. Li, J. Chen, S. Cai, Z. Long, X. S. Fang, *Adv. Funct. Mater.* **2018**, *28*, 1802029.
- [42] F. Wang, T. Gao, Q. Zhang, Z. Y. Hu, B. Jin, L. Li, X. Zhou, H. Li, G. Van Tendeloo, T. Zhai, *Adv. Mater.* **2019**, *31*, 1806306.
- [43] M. Liao, L. Sang, T. Teraji, M. Imura, J. Alvarez, Y. Koide, *Jpn. J. Appl. Phys.* **2012**, *51*, 090115.
- [44] T. Yang, S. Chen, X. Li, X. Xu, F. Gao, L. Wang, J. Chen, W. Yang, X. Hou, X. S. Fang, *Adv. Funct. Mater.* **2019**, *29*, 1806250.
- [45] H. Wang, X. Wang, X. Luo, W. Song, J. Guo, Y. Sun, B. Zhang, L. Wang, X. Zhang, L. He, K. Zhang, S. Li, *ACS Photonics* **2019**, *6*, 1972.
- [46] A. A. Ahmed, M. Devarajan, N. Afzal, *Sens. Actuators, A* **2017**, 262, 78.
- [47] Y. Li, Y. Song, Y. Jiang, M. Hu, Z. Pan, X. Xu, H. Chen, Y. Li, L. Hu, X. S. Fang, *Adv. Funct. Mater.* **2017**, *27*, 1701066.
- [48] C.-Y. Tsay, C.-L. Chen, *J. Cryst. Growth* **2017**, 468, 662.
- [49] Z. Xu, L. Han, B. Lou, X. Zhang, S. Dong, *J. Mater. Chem. C* **2014**, *2*, 2470.
- [50] Z. Xu, L. Han, B. Lou, X. Zhang, S. Dong, *Nanoscale* **2014**, *6*, 145.
- [51] M. Li, J. Zhang, H. Gao, F. Li, S.-E. Lindquist, N. Wu, R. Wang, *ACS Appl. Mater. Interfaces* **2016**, *8*, 6662.
- [52] W. X. Ouyang, L. Su, X. S. Fang, *Small* **2018**, *14*, 1801611.
- [53] W. Tu, T. Liu, Z. Zhang, G. Wu, H. Chen, M. Wang, *Synth. Met.* **2016**, 219, 20.
- [54] J. B. Wang, W. L. Li, B. Chu, L. L. Chen, G. Zhang, Z. S. Su, Y. R. Chen, D. F. Yang, J. Z. Zhu, S. H. Wu, *Org. Electron.* **2010**, *11*, 1301.
- [55] X. Gong, M. Tong, Y. Xia, W. Cai, J. S. Moon, Y. Cao, G. Yu, C.-L. Shieh, B. Nilsson, A. J. Heeger, *Science* **2009**, 325, 1665.

- [56] C. Liu, L. Wang, M. Liu, C. Li, C. Li, G. Che, B. Su, *Chem. Res. Chin. Univ.* **2012**, *28*, 503.
- [57] W. Tian, H. Zhou, L. Li, *Small* **2017**, *13*, 1702107.
- [58] S. Han, Y. Yao, X. Liu, B. Li, C. Ji, Z. Sun, M. Hong, J. Luo, *Small* **2019**, *15*, 1901194.
- [59] D. Ghoshal, T. Wang, H. Z. Tsai, S. W. Chang, M. Crommie, N. Koratkar, S. F. Shi, *Adv. Opt. Mater.* **2019**, *7*, 1900039.
- [60] Y. Chen, M. He, J. Peng, Y. Sun, Z. Liang, *Adv. Sci.* **2016**, *3*, 1500392.
- [61] H. Wang, D. H. Kim, *Chem. Soc. Rev.* **2017**, *46*, 5204.
- [62] V. Adinolfi, O. Ouellette, M. I. Saidaminov, G. Walters, A. L. Abdelhady, O. M. Bakr, E. H. Sargent, *Adv. Mater.* **2016**, *28*, 7264.
- [63] G. Maculan, A. D. Sheikh, A. L. Abdelhady, M. I. Saidaminov, M. A. Haque, B. Murali, E. Alarousu, O. F. Mohammed, T. Wu, O. M. Bakr, *J. Phys. Chem. Lett.* **2015**, *6*, 3781.
- [64] Y. Zhang, Y. Liu, Z. Xu, H. Ye, Q. Li, M. Hu, Z. Yang, S. Liu, *J. Mater. Chem. C* **2019**, *7*, 1584.
- [65] F. Yan, Z. Wei, X. Wei, Q. Lv, W. Zhu, K. Wang, *Small Methods* **2018**, *2*, 1700349.
- [66] C. Gong, K. Hu, X. Wang, P. Wangyang, C. Yan, J. Chu, M. Liao, L. Dai, T. Zhai, C. Wang, L. Li, J. Xiong, *Adv. Funct. Mater.* **2018**, *28*, 1706559.
- [67] J. D. Yao, Z. Q. Zheng, G. W. Yang, *Prog. Mater. Sci.* **2019**, *106*, 100573.
- [68] F. Wang, Z. Wang, T. A. Shifa, Y. Wen, F. Wang, X. Zhan, Q. Wang, K. Xu, Y. Huang, L. Yin, C. Jiang, J. He, *Adv. Funct. Mater.* **2017**, *27*, 1603254.
- [69] X. Zhou, Q. Zhang, L. Gan, H. Li, J. Xiong, T. Zhai, *Adv. Sci.* **2016**, *3*, 1600177.
- [70] Q. Zhang, X. Li, Z. He, M. Xu, C. Jin, X. Zhou, *J. Phys. D: Appl. Phys.* **2019**, *52*, 303002.
- [71] Y. Yan, W. Xiong, S. Li, K. Zhao, X. Wang, J. Su, X. Song, X. Li, S. Zhang, H. Yang, X. Liu, L. Jiang, T. Zhai, C. Xia, J. Li, Z. Wei, *Adv. Opt. Mater.* **2019**, *7*, 1900622.
- [72] Y. Yang, S. C. Liu, X. Wang, Z. Li, Y. Zhang, G. Zhang, D. J. Xue, J. S. Hu, *Adv. Funct. Mater.* **2019**, *29*, 1900411.
- [73] H. Xiao, T. Liang, M. Xu, *Small* **2019**, *15*, 1901767.
- [74] R. Jiang, B. Li, C. Fang, J. Wang, *Adv. Mater.* **2014**, *26*, 5274.
- [75] X. Li, J. Zhu, B. Wei, *Chem. Soc. Rev.* **2016**, *45*, 3145.
- [76] K. Hu, H. Chen, M. Jiang, F. Teng, L. Zheng, X. S. Fang, *Adv. Funct. Mater.* **2016**, *26*, 6641.
- [77] F. Barati, M. Grossnickle, S. Su, R. K. Lake, V. Aji, N. M. Gabor, *Nat. Nanotechnol.* **2017**, *12*, 1134.
- [78] A. J. Nozik, *Nat. Nanotechnol.* **2009**, *4*, 548.
- [79] O. E. Semonin, J. M. Luther, S. Choi, H.-Y. Chen, J. Gao, A. J. Nozik, M. C. Beard, *Science* **2011**, *334*, 1530.
- [80] A. P. Litvin, I. V. Martynenko, F. Purcell-Milton, A. V. Baranov, A. V. Fedorov, Y. K. Gun'ko, *J. Mater. Chem. A* **2017**, *5*, 13252.
- [81] R. D. Schaller, V. M. Agranovich, V. I. Klimov, *Nat. Phys.* **2005**, *1*, 189.
- [82] D. Ghosh, S. Kapri, S. Bhattacharyya, *ACS Appl. Mater. Interfaces* **2016**, *8*, 35496.
- [83] B. Zhou, B. Shi, D. Jin, X. Liu, *Nat. Nanotechnol.* **2015**, *10*, 924.
- [84] T. Zou, X. Liu, R. Qiu, Y. Wang, S. Huang, C. Liu, Q. Dai, H. Zhou, *Adv. Opt. Mater.* **2019**, *7*, 1801812.
- [85] X. Liu, X. Ji, M. Liu, N. Liu, Z. Tao, Q. Dai, L. Wei, C. Li, X. Zhang, B. Wang, *ACS Appl. Mater. Interfaces* **2015**, *7*, 2452.
- [86] K. Sarkar, M. Hossain, P. Devi, K. D. M. Rao, P. Kumar, *Adv. Mater. Interfaces* **2019**, *6*, 1900923.
- [87] N. Prakash, G. Kumar, M. Singh, S. P. Singh, B. Satpati, S. P. Khanna, P. Pal, *Adv. Opt. Mater.* **2019**, *7*, 1900340.
- [88] D. Shao, H. Sun, J. Gao, G. Xin, M. A. Aguilar, T. Yao, N. Koratkar, J. Lian, S. Sawyer, *Nanoscale* **2014**, *6*, 13630.
- [89] S. Zheng, J. Lu, X. Duan, *ACS Omega* **2016**, *1*, 1239.
- [90] L. X. Zheng, P. Yu, K. Hu, F. Teng, H. Chen, X. S. Fang, *ACS Appl. Mater. Interfaces* **2016**, *8*, 33924.
- [91] M. Wang, Y. Lian, X. Wang, *Curr. Appl. Phys.* **2009**, *9*, 189.
- [92] S.-W. Lee, S.-H. Cha, K.-J. Choi, B.-H. Kang, J.-S. Lee, S.-W. Kim, J.-S. Kim, H.-M. Jeong, S.-A. Gopalan, D.-H. Kwon, S.-W. Kang, *Sensors* **2016**, *16*, 74.
- [93] P. P. Yu, K. Hu, H. Chen, L. Zheng, X. S. Fang, *Adv. Funct. Mater.* **2017**, *27*, 1703166.
- [94] J. Mallows, M. Planells, V. Thakare, R. Bhosale, S. Ogale, N. Robertson, *ACS Appl. Mater. Interfaces* **2015**, *7*, 27597.
- [95] M. Garg, B. R. Tak, V. R. Rao, R. Singh, *ACS Appl. Mater. Interfaces* **2019**, *11*, 12017.
- [96] X. Zhang, J. Li, W. Yang, B. Leng, P. Niu, X. Jiang, B. Liu, *ACS Appl. Mater. Interfaces* **2019**, *11*, 24459.
- [97] R. Marschall, *Adv. Funct. Mater.* **2014**, *24*, 2421.
- [98] W. X. Ouyang, F. Teng, X. S. Fang, *Adv. Funct. Mater.* **2018**, *28*, 1707178.
- [99] F. Teng, L. Zheng, K. Hu, H. Chen, Y. Li, Z. Zhang, X. S. Fang, *J. Mater. Chem. C* **2016**, *4*, 8416.
- [100] L. X. Su, W. Yang, J. Cai, H. Chen, X. S. Fang, *Small* **2017**, *13*, 1701687.
- [101] X. Wu, J. Dai, Y. Zhao, Z. Zhuo, J. Yang, X. C. Zeng, *ACS Nano* **2012**, *6*, 7443.
- [102] J. Xu, Y. Chang, L. Gan, Y. Ma, T. Zhai, *Adv. Sci.* **2015**, *2*, 1500023.
- [103] A. Aldalbahi, M. Rivera, M. Rahaman, A. Zhou, W. M. Alzuraiqi, P. Feng, *Nanomaterials* **2017**, *7*, 454.
- [104] K. Ahmed, R. Dahal, A. Weltz, J. Q. Lu, Y. Danon, I. B. Bhat, *Appl. Phys. Lett.* **2016**, *109*, 113501.
- [105] C. Chen, Y. Ma, J. Chen, H. San, *J. Mater. Sci.* **2018**, *53*, 12455.
- [106] J. Cai, P. Ruffieux, R. Jaafar, M. Bieri, T. Braun, S. Blankenburg, M. Muoth, A. P. Seitsonen, M. Saleh, X. Feng, K. Müllen, R. Fasel, *Nature* **2010**, *466*, 470.
- [107] S. Thangavel, K. Krishnamoorthy, V. Krishnaswamy, N. Raju, S. J. Kim, G. Venugopal, *J. Phys. Chem. C* **2015**, *119*, 22057.
- [108] Z. Jin, Q. Zhou, Y. Chen, P. Mao, H. Li, H. Liu, J. Wang, Y. Li, *Adv. Mater.* **2016**, *28*, 3697.
- [109] H. Liu, A. T. Neal, Z. Zhu, Z. Luo, X. Xu, D. Tománek, P. D. Ye, *ACS Nano* **2014**, *8*, 4033.
- [110] L. Li, Y. Yu, G. J. Ye, Q. Ge, X. Ou, H. Wu, D. Feng, X. H. Chen, Y. Zhang, *Nat. Nanotechnol.* **2014**, *9*, 372.
- [111] Y. Wang, C. Cong, R. Fei, W. Yang, Y. Chen, B. Cao, L. Yang, T. Yu, *Nano Res.* **2015**, *8*, 3944.
- [112] S. Cao, Y. Xing, J. Han, X. Luo, W. Lv, W. Lv, B. Zhang, Z. Zeng, *Nanoscale* **2018**, *10*, 16805.
- [113] L.-B. Luo, X.-B. Yang, F.-X. Liang, J.-S. Jie, Q. Li, Z.-F. Zhu, C.-Y. Wu, Y.-Q. Yu, L. Wang, *CrystEngComm* **2012**, *14*, 1942.
- [114] K. Hu, F. Teng, L. Zheng, P. Yu, Z. Zhang, H. Chen, X. S. Fang, *Laser Photonics Rev.* **2017**, *11*, 1600257.
- [115] L. X. Zheng, K. Hu, F. Teng, X. S. Fang, *Small* **2017**, *13*, 1602448.
- [116] S. Noothongkaew, O. Thumthan, K.-S. An, *Mater. Lett.* **2018**, *233*, 318.
- [117] L. X. Zheng, F. Teng, Z. Zhang, B. Zhao, X. S. Fang, *J. Mater. Chem. C* **2016**, *4*, 10032.
- [118] T. Xie, G. Liu, B. Wen, J. Y. Ha, N. V. Nguyen, A. Motayed, R. Debnath, *ACS Appl. Mater. Interfaces* **2015**, *7*, 9660.
- [119] P. Hu, L. Wang, M. Yoon, J. Zhang, W. Feng, X. Wang, Z. Wen, J. C. Idrobo, Y. Miyamoto, D. B. Geohegan, K. Xiao, *Nano Lett.* **2013**, *13*, 1649.
- [120] G. Chen, Y. Yu, K. Zheng, T. Ding, W. Wang, Y. Jiang, Q. Yang, *Small* **2015**, *11*, 2848.
- [121] Q. Yun, L. Li, Z. Hu, Q. Lu, B. Chen, H. Zhang, *Adv. Mater.* **2019**, *31*, 1903826.
- [122] Y.-H. Lee, X.-Q. Zhang, W. Zhang, M.-T. Chang, C.-T. Lin, K.-D. Chang, Y.-C. Yu, J. T.-W. Wang, C.-S. Chang, L.-J. Li, T.-W. Lin, *Adv. Mater.* **2012**, *24*, 2320.

- [123] Y. Zhang, Y. Zhang, Q. Ji, J. Ju, H. Yuan, J. Shi, T. Gao, D. Ma, M. Liu, Y. Chen, X. Song, H. Y. Hwang, Y. Cui, Z. Liu, *ACS Nano* **2013**, *7*, 8963.
- [124] X. Wang, Y. Gong, G. Shi, W. L. Chow, K. Keyshar, G. Ye, R. Vajtai, J. Lou, Z. Liu, E. Ring, B. K. Tay, P. M. Ajayan, *ACS Nano* **2014**, *8*, 5125.
- [125] H. Fang, S. Chuang, T. C. Chang, K. Takei, T. Takahashi, A. Javey, *Nano Lett.* **2012**, *12*, 3788.
- [126] T. J. Octon, V. K. Nagareddy, S. Russo, M. F. Craciun, C. D. Wright, *Adv. Opt. Mater.* **2016**, *4*, 1750.
- [127] Y. Yi, C. Wu, H. Wang, H. Liu, H. Li, H. Zhang, H. He, J. Wang, *Solid State Commun.* **2017**, *260*, 45.
- [128] X. Zhao, X. Zhang, T. Wang, S. Wei, L. Yang, *J. Alloys Compd.* **2018**, *748*, 798.
- [129] Y. H. Huang, R. S. Chen, J. R. Zhang, Y. S. Huang, *Nanoscale* **2015**, *7*, 18964.
- [130] Y. Wang, Y. Li, Z. Chen, *J. Mater. Chem. C* **2015**, *3*, 9603.
- [131] L. Pi, L. Li, K. Liu, Q. Zhang, H. Li, T. Zhai, *Adv. Funct. Mater.* **2019**, *29*, 1904932.
- [132] E. Butanovs, S. Vlassov, A. Kuzmin, S. Piskunov, J. Butikova, B. Polyakov, *ACS Appl. Mater. Interfaces* **2018**, *10*, 13869.
- [133] R. Zhuo, L. Zeng, H. Yuan, D. Wu, Y. Wang, Z. Shi, T. Xu, Y. Tian, X. Li, Y. H. Tsang, *Nano Res.* **2019**, *12*, 183.
- [134] X. J. Xu, J. Chen, S. Cai, Z. Long, Y. Zhang, L. Su, S. He, C. Tang, P. Liu, H. Peng, X. S. Fang, *Adv. Mater.* **2018**, *30*, 1803165.
- [135] Y. Zhang, W. Xu, X. Xu, J. Cai, W. Yang, X. S. Fang, *J. Phys. Chem. Lett.* **2019**, *10*, 836.
- [136] A. Jain, O. Voznyy, S. Hoogland, M. Korkusinski, P. Hawrylak, E. H. Sargent, *Nano Lett.* **2016**, *16*, 6491.
- [137] J. Song, J. Yuan, F. Xia, J. Liu, Y. Zhang, Y. L. Zhong, J. Zheng, Y. Liu, S. Li, M. Zhao, Z. Tian, R. A. Caruso, K. P. Loh, Q. Bao, *Adv. Electron. Mater.* **2016**, *2*, 1600077.
- [138] L. Su, Q. Zhang, T. Wu, M. Chen, Y. Su, Y. Zhu, R. Xiang, X. Gui, Z. Tang, *Appl. Phys. Lett.* **2014**, *105*, 072106.
- [139] T. N. Oder, J. Li, J. Y. Lin, H. X. Jiang, *Appl. Phys. Lett.* **2000**, *77*, 791.
- [140] B. Zhao, F. Wang, H. Chen, L. Zheng, L. Su, D. Zhao, X. S. Fang, *Adv. Funct. Mater.* **2017**, *27*, 1700264.
- [141] M. Chen, B. Zhao, G. Hu, X. S. Fang, H. Wang, L. Wang, J. Luo, X. Han, X. Wang, C. Pan, Z. L. Wang, *Adv. Funct. Mater.* **2018**, *28*, 1706379.
- [142] B. W. Li, M. Osada, T. C. Ozawa, Y. Ebina, K. Akatsuka, R. Ma, H. Funakubo, T. Sasaki, *ACS Nano* **2010**, *4*, 6673.
- [143] M. Osada, T. Sasaki, *Adv. Mater.* **2012**, *24*, 210.
- [144] J. Chu, F. Wang, L. Yin, L. Lei, C. Yan, F. Wang, Y. Wen, Z. Wang, C. Jiang, L. Feng, J. Xiong, Y. Li, J. He, *Adv. Funct. Mater.* **2017**, *27*, 1701342.
- [145] C. Gong, J. Chu, C. Yin, C. Yan, X. Hu, S. Qian, Y. Hu, K. Hu, J. Huang, H. Wang, Y. Wang, P. Wangyang, T. Lei, L. Dai, C. Wu, B. Chen, C. Li, M. Liao, T. Zhai, J. Xiong, *Adv. Mater.* **2019**, *31*, 1903580.
- [146] M. Gong, Q. Liu, B. Cook, B. Kattel, T. Wang, W. L. Chan, D. Ewing, M. Casper, A. Stramel, J. Z. Wu, *ACS Nano* **2017**, *11*, 4114.
- [147] W. Yang, J. X. Chen, Y. Zhang, Y. Zhang, J. H. He, X. S. Fang, *Adv. Funct. Mater.* **2019**, *29*, 1808182.
- [148] A. K. Geim, I. V. Grigorieva, *Nature* **2013**, *499*, 419.
- [149] M. Gong, Q. Liu, R. Goul, D. Ewing, M. Casper, A. Stramel, A. Elliot, J. Z. Wu, *ACS Appl. Mater. Interfaces* **2017**, *9*, 27801.
- [150] M. Gong, R. Sakidja, Q. Liu, R. Goul, D. Ewing, M. Casper, A. Stramel, A. Elliot, J. Z. Wu, *Adv. Opt. Mater.* **2018**, *6*, 1701241.
- [151] D. Zhang, W. Zheng, R. Lin, Y. Li, F. Huang, *Adv. Funct. Mater.* **2019**, *29*, 1900935.
- [152] W. Peng, X. Wang, R. Yu, Y. Dai, H. Zou, A. C. Wang, Y. He, Z. L. Wang, *Adv. Mater.* **2017**, *29*, 1606698.
- [153] Z. M. Zhang, Y. Ning, X. S. Fang, *J. Mater. Chem. C* **2019**, *7*, 223.
- [154] A. K. Rana, J. T. Park, J. Kim, C.-P. Wong, *Nano Energy* **2019**, *64*, 103952.
- [155] P. Ghamgosar, F. Rigoni, S. You, I. Dobryden, M. G. Kohan, A. L. Pellegrino, I. Concina, N. Almqvist, G. Malandrino, A. Vomiero, *Nano Energy* **2018**, *51*, 308.
- [156] C. Liu, M. Peng, A. Yu, J. Liu, M. Song, Y. Zhang, J. Zhai, *Nano Energy* **2016**, *26*, 417.
- [157] T. Ji, Q. Liu, R. Zou, Y. Sun, K. Xu, L. Sang, M. Liao, Y. Koide, L. Yu, J. Hu, *Adv. Funct. Mater.* **2016**, *26*, 1400.
- [158] M. Wei, K. Yao, Y. Liu, C. Yang, X. Zang, L. Lin, *Small* **2017**, *13*, 1701328.
- [159] S. Chen, X. Liu, X. Qiao, X. Wan, K. Shehzad, X. Zhang, Y. Xu, X. Fan, *Small* **2017**, *13*, 1604033.
- [160] D. Bessinger, L. Ascherl, F. Auras, T. Bein, *J. Am. Chem. Soc.* **2017**, *139*, 12035.
- [161] R. Nie, X. Deng, L. Feng, G. Hu, Y. Wang, G. Yu, J. Xu, *Small* **2017**, *13*, 1603260.
- [162] M. A. Juntunen, J. Heinonen, V. Vähänissi, P. Repo, D. Valluru, H. Savin, *Nat. Photonics* **2016**, *10*, 777.
- [163] Z. Wang, R. Yu, X. Wang, W. Wu, Z. L. Wang, *Adv. Mater.* **2016**, *28*, 6880.
- [164] Y. Zhang, X. Zhao, J. Chen, S. Li, W. Yang, X. S. Fang, *Adv. Funct. Mater.* **2020**, *30*, 1907650.
- [165] P. Wang, H. Xia, Q. Li, F. Wang, L. Zhang, T. Li, P. Martyniuk, A. Rogalski, W. Hu, *Small* **2019**, *15*, 1904396.
- [166] P. Wang, Y. Wang, L. Ye, M. Wu, R. Xie, X. Wang, X. Chen, Z. Fan, J. Wang, W. Hu, *Small* **2018**, *14*, 1800492.
- [167] D. Zheng, H. Fang, P. Wang, W. Luo, F. Gong, J. C. Ho, X. Chen, W. Lu, L. Liao, J. Wang, W. Hu, *Adv. Funct. Mater.* **2016**, *26*, 7690.
- [168] L. Li, Y. Zhang, R. Wang, J. Sun, Y. Si, H. Wang, C. Pan, Y. Dai, *Nano Energy* **2019**, *65*, 104046.
- [169] J. Zhou, L. Chen, Y. Wang, Y. He, X. Pan, E. Xie, *Nanoscale* **2016**, *8*, 50.
- [170] X. Li, C. Gao, H. Duan, B. Lu, Y. Wang, L. Chen, Z. Zhang, X. Pan, E. Xie, *Small* **2013**, *9*, 2005.
- [171] Y. Wang, L. Chen, H. Zhou, K. Wei, Z. Zhu, E. Xie, W. Cao, W. Han, *J. Mater. Chem. C* **2019**, *7*, 8011.
- [172] Y. Dong, Y. Zou, J. Song, Z. Zhu, J. Li, H. Zeng, *Nano Energy* **2016**, *30*, 173.
- [173] L. Li, L. Gu, Z. Lou, Z. Fan, G. Shen, *ACS Nano* **2017**, *11*, 4067.
- [174] Y. Zhang, S. Y. Li, W. Yang, M. K. Joshi, X. S. Fang, *J. Phys. Chem. Lett.* **2019**, *10*, 2400.
- [175] Z. M. Zhang, X. S. Fang, *J. Inorg. Mater.* **2019**, *34*, 991.
- [176] Z. H. Long, X. J. Xu, W. Yang, M. X. Hu, D. V. Shtansky, D. Golberg, X. S. Fang, *Adv. Electron. Mater.* **2020**, *6*, 1901048.